OBJECT DETECTION FROM REGISTERED VISUAL AND INFRARED SEQUENCES WITH THE HELP OF ACTIVE CONTOURS

A THESIS SUBMITTED TO
THE GRADUATE SCHOOL OF NATURAL AND APPLIED SCIENCES
OF
MIDDLE EAST TECHNICAL UNIVERSITY

BY

HÜSEYİN YÜRÜK

IN PARTIAL FULLFILLMENT OF THE REQUIREMENTS
FOR
THE DEGREE OF MASTER OF SCIENCE
IN
ELECTRICAL AND ELECTRONICS ENGINEERING

JULY 2008

Approval of the thesis:

OBJECT DETECTION FROM REGISTERED VISUAL AND INFRARED SEQUENCES WITH THE HELP OF ACTIVE CONTOURS

submitted by **HÜSEYİN YÜRÜK** in partial fulfillment of the requirements for the degree of **Master of Science in Electrical and Electronics Engineering Department, Middle East Technical University** by,

Prof. Dr. Canan Özgen _____
Dean, Graduate School of **Natural and Applied Sciences**

Prof. Dr. İsmet Erkmen _____
Head of Department, **Electrical and Electronics Engineering**

Assist. Prof. Dr. İlkay Ulusoy _____
Supervisor, **Electrical and Electronics Engineering Dept., METU**

Examining Committee Members:

Prof. Dr. Uğur HALICI _____
Electrical and Electronics Engineering Dept., METU

Assist. Prof. Dr. İlkay Ulusoy _____
Electrical and Electronics Engineering Dept., METU

Prof. Dr. Gözde Bozdağı Akar _____
Electrical and Electronics Engineering Dept., METU

Assist. Prof. Dr. Alptekin Temizel _____
Informatics Institute, METU

MSc. İlker Gürel _____
ASELSAN Inc.

Date: _____

I hereby declare that all information in this document has been obtained and presented in accordance with academic rules and ethical conduct. I also declare that, as required by these rules and conduct, I have fully cited and referenced all material and results that are not original to this work.

Name, Last name : Hüseyin YÜRÜK

Signature :

ABSTRACT

OBJECT DETECTION FROM REGISTERED VISUAL AND INFRARED SEQUENCES WITH THE HELP OF ACTIVE CONTOURS

Yürük, Hüseyin

M. S., Department of Electrical and Electronics Engineering
Supervisor : Assist. Prof. Dr. İlkay Ulusoy

July 2008, 82 pages

Robust object detection from registered infrared and visible image streams is proposed for outdoor surveillance. In doing this, halo effect in infrared images is used as a benefit to extract object boundary by fitting active contour models (snake) to the foreground regions where these regions are detected by using the useful information from both visual and infrared domains together.

Synchronization and registration are performed for each infrared and visible image couple. Various background modeling methods such as Single Gaussian, Non-Parametric and Mixture of Gaussian models are implemented. For Single Gaussian and Mixture of Gaussian background modeling, infrared, color intensity and color channels domains are modelled separately. First of all, background subtraction is applied in the infrared domain in order to find the initial foreground regions and these are used as a mask for the foreground detection in the visible domain. After removing the shadows from the foreground regions in the visible domain, pixel-wise OR operation is applied between the foreground regions of the infrared and

visible couple and the final foreground mask is formed. For Non-Parametric background modeling, all domains are used altogether to extract foreground regions. For all background modelling methods, the resulting mask is used to get the final foreground regions in the infrared image. Finally, snake is applied to each connected component of the foreground regions on the infrared image for the purpose of object detection.

Two datasets are used to demonstrate our results for human detection where comparisons against manually segmented human regions and against other results in the literature are presented.

Keywords : Background modeling, shadow detection, fusion of infrared and color domain, application of snake algorithm

ÖZ

AKTİF KONTURLAR YARDIMIYLA, BIRBIRIYLE UYUMLANMIŞ RENKLİ VE KIZIL ÖTESİ DİZİLERİNDEN NESNELERIN BULUNMASI

Yürük, Hüseyin

Yüksek Lisans, Elektrik Elektronik Mühendisliği Bölümü
Tez Yöneticisi :Dr. İlkay Ulusoy

Temmuz 2008, 82 sayfa

Bu tez kapsamında, dış alan güvenliği için birbiriyle uyumlanmış kızıl ötesi ve renkli görüntü dizilerinden sağlam nesne bulunması önerilmiştir. Bu işi gerçekleştirmek için, kızıl ötesinde bulunan "halo" etkisi, bir avantaj olarak, nesnelerin sınırlarının, aktif kontur modellerin ön plan alanlarına uyarlanarak çıkartılmasında kullanılmıştır. Ön plan, kızıl ötesi ve renkli alanlardan elde edilen kullanışlı bilgilerin kullanılmasıyla bulunmaktadır.

Her bir kızıl ötesi ve renkli resim çifti için eşleme ve uyumlama işlemi gerçekleştirilmektedir. Tekli Gaussian, parametrik olmayan ve karma Gaussian modelleri gibi, bir çok arka plan modelleme metotları uygulanmıştır. Tekli ve karışım Gaussian arka plan modelleri için, arka plan istatistiksel olarak her bir kızıl ötesi, renk yoğunluğu ve kanalları alanında ayrı ayrı modellenmiştir. Arka plan çıkarma işlemi ilk olarak kızıl ötesi alanda, ön planın çıkarılması için yapılmış ve bu bölge renkli alanlarda arka plan çıkarma işleminde maske olarak kullanılmıştır. Renkli alanın ön planında bulunan gölgeler çıkarıldıktan sonra, son maske, kızıl

ötesi ve renkli çiftin ön plan bölgelerine, piksel bazında “veya” işlemi uygulanması ile oluşturulur. Parametrik olmayan model için, bütün alanlar ön plan alanlarının çıkartılması için birlikte kullanılmıştır. Bütün arka plan modelleme metotları için, sonuçta oluşan maske, kızıl ötesi resimden ilgili bölgelerin elde edilmesi amacıyla kullanılmaktadır. Son olarak, nesne bulunması amacıyla, kızıl ötesi resmindeki bulunan ön plan bölgelerinden her bir bağlı parçasına “snake” algoritması uygulanır.

İnsan bulma için elde ettiğimiz sonuçları göstermek amacıyla iki veri kümesi kullanılmıştır. El il insan nesnesi bölgeleri ve ayrıca literatürde bulunan diğer sonuçlar ile kıyaslamalar sunulmuştur.

Anahtar Kelimeler : Arka plan modelleme, gölge bulma, kızıl ötesi ve renkli alanların birleştirilmesi, “snake” algoritmasının uygulanması

To My Wife

ACKNOWLEDGEMENTS

I would like to express my gratitude to my supervisor Dr. İlkay Ulusoy for her guidance, advice, criticism, encouragement and insight throughout the completion of the thesis.

I am indebted to all of my friends and colleagues for their support and encouragements. I am also grateful to ASELSAN Inc. for the facilities that made my work easier.

Finally I am grateful to my wife for her continuous support and encouragements.

TABLE OF CONTENTS

ABSTRACT ..... **IV**

ÖZ ..... **VI**

ACKNOWLEDGEMENTS ..... **IX**

TABLE OF CONTENTS ..... **X**

LIST OF TABLES ..... **XII**

LIST OF FIGURES ..... **XIII**

LIST OF ABBREVIATIONS ..... **XVII**

CHAPTER

1 INTRODUCTION **1**

2 AN OVERVIEW OF RELATED WORKS **3**

2.1 ALGORITHMS WHICH USE BOTH INFRARED AND VISIBLE IMAGE 3

2.1.1 Image Registration 4

2.1.2 Background Modelling 4

2.1.3 Foreground Detection 6

2.1.4 Fusion of Infrared and Visible Images 7

2.2 ALGORITHMS WHICH USE INFRARED OR VISIBLE IMAGE 8

2.3 ALGORITHMS WHICH USE ONLY INFRARED IMAGE 8

2.4 ALGORITHMS WHICH USE ONLY VISIBLE IMAGE 10

2.5 ALGORITHMS FOR SHADOW DETECTION 11

3 APPLIED METHODS **13**

3.1 IMAGE REGISTRATION 13

3.2 BACKGROUND MODELING 16

3.2.1 Single Gaussian Model: Infrared, Color Intensity, Color Channels Separately 16

3.2.2 Single Gaussian Model: Infrared and Color Intensity as One Vector 18

3.2.3 Single Gaussian Model: Infrared and Color Channels as One Vector 18

3.2.4 Single Gaussian Model: Infrared, Color Intensity and Color Channels as One Vector ... 19

3.2.5 Non-Parametric Model 19
3.2.6 Non-Parametric Model: Infrared and Color Separately 28
3.2.7 Mixture of K Gaussian Model 28
3.3 FOREGROUND DETECTION 31
3.3.1 Foreground Detection Based on Single Gaussian Background Model 31
3.3.2 Foreground Detection Based on Non-Parametric Background Model 34
3.3.3 Foreground Detection Based on Mixture of Gaussian Background Model 36
3.3.4 Shadow Detection 37
3.3.5 Fusion of Infrared and Visible Domains 42
3.4 APPLICATION OF SNAKE ALGORITHM 45

4 EXPERIMENTAL RESULTS 50

4.1 EXPERIMENTAL SETUP 50
4.2 BACKGROUND MODELLING 52
4.3 FOREGROUND DETECTION 53
4.3.1 Fusion of Infrared and Visible Domain 58
4.4 APPLICATION OF SNAKE 59
4.5 PERFORMANCE FOR THE WHOLE ALGORITHM 60

5 SUMMARY AND CONCLUSIONS 77

REFERENCES 79

LIST OF TABLES

Table 4-1 Comparison of Results: Our Algorithm (Based on Kinds of Background Modelling) and Reference [1] 65
Table 4-2 Results of Our Algorithm Based on Single Gaussian Methods (Combination of Bands as One Vector) and Reference [1]..... 70
Table 4-3 Results of Our Algorithm: Based on Several Kinds of Background Models Obtained by Using Our Dataset..... 72
Table 4-4 Results of Based on Single Gaussian Methods (Combination of Bands as One Vector) Obtained by Using Our Dataset..... 75

LIST OF FIGURES

Figure 3-1 Infrared and Visible Image at Frame Number 1463 and 1400 Respectively 14
Figure 3-2 Addition of Original Images of Infrared and Color Domain..... 14
Figure 3-3 Registered Infrared and Visible Image..... 15
Figure 3-4 Addition of Registered Images of Infrared and Color Domain..... 15
Figure 3-5 Mean Images of Infrared, Color Intensity and Color Channels of Single Gaussian Background Method 18
Figure 3-6 Infrared Frame 5 of Sequence1 of OTCBVS Dataset 22
Figure 3-7 First and Fifth Iteration of Anisotropic Diffusion Respectively 22
Figure 3-8 Fifth Iteration of Gaussian Filter..... 23
Figure 3-9 Non-Pedestrian Detection and Meaning of Colors 25
Figure 3-10 Output of Rough Pedestrian Detection and Dilation Operation..... 25
Figure 3-11 Likelihood Image of the Non-Parametric Method 28
Figure 3-12 Mean Images of Infrared, Color Intensity and Color Channels of Mixture of Gaussian Background Method 31
Figure 3-13 Current Infrared, Color Intensity and Color Channels Image (Frame 803 of Sequence4 of the OTCBVS Dataset)..... 32
Figure 3-14 Foreground Regions of Infrared, Color Intensity and Color Channels (without Masked by Infrared Foreground)..... 33
Figure 3-15 Foreground Regions of Color Intensity and Color Channels (with Masked by Infrared Foreground) 33
Figure 3-16 Foreground Regions of Single Gaussian Methods (Combination of Bands as One Vector)..... 34
Figure 3-17 Foreground Regions of Non-Parametric Method..... 35
Figure 3-18 Foreground Regions of Infrared and LUV (without Masked by Infrared Foreground)..... 36
Figure 3-19 Foreground Regions of LUV (with Masked by Infrared Foreground). 36

Figure 3-20 Foreground Regions of Infrared, Color Intensity and Color Channels (without Masked by Infrared Foreground) 37
Figure 3-21 Foreground Regions of Color Intensity and Color Channels (with Masked by Infrared Foreground) 37
Figure 3-22 Frame 319 of Sequence2 of the OTCBVS Dataset for Shadow Detection 38
Figure 3-23 Shadow Detection Results for Method-1, Originally Shadow Image and Final Shadow Image After Masked with Foreground Region of Color Image ... 39
Figure 3-24 Shadow Detection Results for Method-2, Originally Shadow Image and Final Shadow Image After Masked with Foreground Region of Color Image ... 40
Figure 3-25 Shadow Detection Results for Method-3, Possible Shadow Image and Final Shadow Image 42
Figure 3-26 Current Infrared, Color Intensity and Color Channels Image (Frame 665 of Sequence3 of the OTCBVS Dataset) 43
Figure 3-27 Foreground Region of Infrared, Foreground Region of Color and Resulting Final Foreground (Based on SG Background Model) 43
Figure 3-28 Foreground Region of Infrared, Foreground Region of Color and Resulting Final Foreground (Based on Non-Param Background Model) 43
Figure 3-29 Foreground Region of Infrared, Foreground Region of Color and Resulting Final Foreground (Based on MOG Background Model) 44
Figure 3-30 Current Infrared, Color Intensity and Color Channels Image (Frame 240 of Sequence4 of the OTCBVS Dataset) 45
Figure 3-31 Final Foreground Regions (Combination of Bands as One Vector of Single Gaussian and Non-Parametric Background Model) 45
Figure 3-32 Current Infrared, Color Intensity and Color Channels Image (Frame 319 of Sequence2 of the OTCBVS Dataset) 49
Figure 3-33 Foreground Region of Infrared, Resulting Final Foreground Region and Application of Snake Algorithm 49
Figure 4-1 Experimental Setup and Place 51
Figure 4-2 Mean Images of Infrared, Color Intensity and Color Channels of Single Gaussian Background Method 52

Figure 4-3 Mean Images of Infrared, Color Intensity and Color Channels of Mixture Gaussian Background Method 53
Figure 4-4 Current Infrared, Color Intensity and Color Channels Image (Frame 373 of Scene2 of Our Dataset) 53
Figure 4-5 Foreground Regions of Infrared, Color Intensity and Color Channels (without Masked by Infrared Foreground) Based on Single Gaussian Background Model..... 54
Figure 4-6 Foreground Regions of Color Intensity and Color Channels (with Masked by Infrared Foreground) Based on Single Gaussian Background Model 54
Figure 4-7 Foreground Regions of Infrared, Color Intensity and Color Channels (without Masked by Infrared Foreground) Based on Mixture of Gaussian Background Model 55
Figure 4-8 Foreground Regions of Color Intensity and Color Channels (with Masked by Infrared Foreground) Based on Mixture of Gaussian Background Model..... 55
Figure 4-9 Foreground Regions of Infrared and LUV (without Masked by Infrared Foreground) Based on Non-Parametric Method 56
Figure 4-10 Foreground Regions of LUV (with Masked by Infrared Foreground) Based on Non-Parametric Method 56
Figure 4-11 Foreground Regions of Non-Parametric Method..... 57
Figure 4-12 Foreground Regions of Single Gaussian Methods (Combination of Bands as One Vector)..... 57
Figure 4-13 Frame 1712 of Scene3 of Our Dataset for Fusion of Infrared and Visible Domain..... 58
Figure 4-14 Completion of Infrared Foreground Regions, Foreground Region of Infrared, Color Domain and Resulting Final Foreground 59
Figure 4-15 Frame 1400 of Scene4 of Our Dataset for Fusion of Infrared and Visible Domain..... 59
Figure 4-16 Foreground Region of Infrared, Resulting Final Foreground Region and Application of Snake Algorithm 60

Figure 4-17 The Block Schema of the Algorithm Based on SG and MOG Background Models 62
Figure 4-18 The Block Schema of the Algorithm Based on Non-Param-1 Background Model 63
Figure 4-19 . The Block Schema of the Algorithm Based on Non-Param-2 Background Model 63
Figure 4-20 Results from Frame 652 of Sequence1 of OTCBVS Dataset 66
Figure 4-21 Results from Frame 442 of Sequence2 of OTCBVS Dataset 66
Figure 4-22 Results from Frame 680 of Sequence3 of OTCBVS Dataset 67
Figure 4-23 Results from Frame 803 of Sequence4 of OTCBVS Dataset 67
Figure 4-24 Results from Frame 508 of Sequence5 in OTCBVS Dataset..... 68
Figure 4-25 Results from Frame 820 of Sequence6 in OTCBVS Dataset..... 68
Figure 4-26 The Block Schema of the Algorithm Based on Single Gaussian where Combinations of each band is modelled as One Vector..... 69
Figure 4-27 Results from Frame 803 of Sequence4 of OTCBVS Dataset 70
Figure 4-28 The Block Schema of the Algorithm Based on SG-IR where Only Infrared Band is Used..... 71
Figure 4-29 Results from Frame 1656 of Scene1 of Our Dataset..... 73
Figure 4-30 Results from Frame 373 of Scene2 of Our Dataset..... 73
Figure 4-31 Results from Frame 300 of Scene3 of Our Dataset..... 73
Figure 4-32 Results from Frame 1400 of Scene4 of Our Dataset..... 74
Figure 4-33 Results from Frame 1834 of Scene5 of Our Dataset..... 74
Figure 4-34 Results from Frame 1876 of Scene6 of Our Dataset..... 74
Figure 4-35 Results from Frame 373 of Scene2 of Our Dataset..... 76

LIST OF ABBREVIATIONS

CSM	Contour Saliency Map
EM	Expectation Maximization
HOG	Histogram of Oriented Gradient
IR	Infrared
MOG	Mixture of Gaussian
Non-Param	Non-Parametric
PCA	Principal Component Analysis
RGB	Red Green Blue
ROI	Region of Interest
SG	Single Gaussian
SVM	Support Vector Machines

CHAPTER 1

INTRODUCTION

Outdoor surveillance has gained a lot of attention in recent years. Outdoor surveillance includes the tasks such as monitoring of sites, critical areas, borders for intrusion or threats from people and vehicles.

The most significant and also desirable feature of the outdoor surveillance systems is their operation all around the day. Color or grayscale video cameras which produce visible spectrum images need an external illumination. This illumination can be provided from the sun light in day time but at night this problem should be solved by artificial illumination. Unfortunately, this solution at night is not always adequate and also not applicable for everywhere. There will still be remaining darker places in which undesirable activities may most likely occur. Infrared spectrum sensors are more suitable and effective for these situations. Infrared cameras produce infrared spectrum images by detecting the amount of thermal radiation emitted/reflected from objects which are at nonzero absolute temperature and can be used both at day and night time. On the other hand, when the temperature of an object is close to the surrounding area, detection of the object becomes more difficult. In these situations, if the color of the object and background is not similar and illumination is available, visual spectrum cameras give more cues which can be used to detect the object. Infrared cameras lack some information such as texture and color which are normally available for visual spectrum cameras. With these complementary properties, using infrared and visible

images together becomes increasingly important in human detection systems in recent years.

The benefits obtained from using infrared and visible images together, come with a question: At which points these sources would be fused? Each information source brings its own unique challenges. Visual spectrum image has problems such as sudden illumination changes, the presence of shadows and poor night time visibility. Infrared image has also problems such as lower signal to noise ratio, polarity inversion and the “halo effect” that appears around hot or cold objects with ferroelectric sensors.

In this study, it is mostly focused on detecting humans. Beneficial information is combined from both visual and thermal images. The proposed approach uses the problem of the halo effect as a benefit to detect objects in infrared images. Snakes are used to obtain the boundary of humans where halo effect helps snakes fit the boundaries easily.

The rest of this paper is organized as follows: in Chapter 2 the related work is summarized. In Chapter 3, the algorithms starting from image registration to snake application are explained. In Chapter 4 experiments and results are demonstrated. In Chapter 5 conclusion and some ideas about future works are given.

CHAPTER 2

AN OVERVIEW OF RELATED WORKS

Object detection from visual and/or infrared images requires some steps of processing such as background modeling, foreground detection and also some post processing in order to extract the clean boundaries of the object.

In this chapter, the related works which include or help for the human detection task are summarized. This chapter is divided into four parts by considering the used source of image. Namely the algorithms are classified as the ones using both infrared and visible image together, the ones using infrared or visible image, the ones using only infrared image and the ones using only visible image. Shadow detection methods are presented also at the end of this chapter.

2.1 Algorithms Which Use both Infrared and Visible Image

Davis and Sharma [1] present a background-subtraction technique which is based on fusion of the contours extracted from thermal and visible image for persistent object detection in urban settings. Conaire *et. al*.[2] present an approach to model background robustly by using data from visible and infrared spectrum. Leykin *et. al*. [4] present a tracking system using information taken from color and thermal cameras and present a method to classify tracked object as a pedestrian or not.

Since each algorithm has a different method for registration, background modeling, foreground detection and fusion of visual and infrared information, these steps are investigated in separate subsections as follows:

2.1.1 Image Registration

In [1], for a particular camera location, a set of corresponding feature points are selected manually from the pair of infrared and visible images. Using this set of points, a homography matrix [17] is constructed to register infrared and visible image pairs.

The camera system used in [2] allows the simultaneous capture of the infrared and visible spectrum video. Temporal alignment is achieved by using the cameras' gen-lock inputs which allow their frame clocks to be synchronized. Spatial alignment is achieved by planar homography. Numerous corresponding points in both domains are selected manually for calculation of homography matrix where least mean squared error is used for optimization.

2.1.2 Background Modelling

In [1], Single Gaussian method is applied to model each background pixel. N frames are captured from both infrared and visible domains to construct proper mean/variance background models. This is done to manage with foreground contained images. Median images of both domains are computed from N images. By using this median image, a weight is computed for each pixel to minimize the effect of the outliers. The statistical background model of each pixel in infrared and intensity component of visible image is constructed by computing weighted means and variances. Mean and covariance model of the normalized color-space component of visible image is computed without weighting parameters. For longer sequences, background model can be updated by using time and update factor.

In [2], non-parametric background model described in [3] is originally used as the background model. Before background modelling, infrared images are pre-processed to get rid of noises. Due to the nature of infrared radiation, hot objects including the device itself emit non-significant amounts of radiation. So infrared images contain high noise and to reduce this noise, anisotropic diffusion is applied to each infrared image. Besides noise removal, before the initialization of the background model, a rough pedestrian detection is made in the infrared image by using size, aspect ratio and thermal features. This detection module has to be very precise and should not miss any pedestrians, so that person pixels are not included into the background model. For each pixel, N samples are stored and are considered to belong to the background distribution. The statistical parameters (mean and variance) of each pixel are calculated separately for 4 bands (L, U, V and infrared). Each background model is updated for the purpose of managing gradual changes in lighting, such as the turning of day to night. This updating is also necessary to include the foreground pixels to the background model which remain static in the scene for some time. Incorrectly labeled foreground regions (such as those caused by changes in brightness rapidly) are also considered as background by this updating.

In [4], multi-model adaptive background model is constructed based on codebook (represented for a single RGB input in [5]). Each pixel in the frame has its own codebook which consists of dynamically growing codewords. In each codeword of that pixel, features are reserved during training frames. For the color input, these features are average pixel value and luminance range. For the thermal input, these features are intensity range occurring at the pixel location. Each codeword also includes a parameter to record the longest interval during the period that the codeword has not occurred. By using this parameter in a learning period, frames can be free of foreground objects.

2.1.3 Foreground Detection

In [1], the squared Mahalanobis distance is used for foreground detection. The result of the distance calculation is thresholded to get foreground pixels. Each threshold value (the infrared, the color intensity and the color channels) is set empirically. Firstly, foreground pixels for an infrared image are found (D^T). Then on the corresponding pair of visible image components, the foreground pixels for intensity and color channels (D_{int} and D_{col} respectively) are found within D^T. Using the D^T as a mask, provides a liberal and generalized thresholding for visible image components which ensures that the detections mostly occur at the desired regions. Extraction of the region of interests (ROIs) of the infrared image is done by applying 5x5 dilation operation and then finding connected components in the D^T. The visible domain ROIs are obtained by pixel-wise union of D_{int} and D_{col} (construct D^V) followed by 5x5 dilation operation.

In [2], the probability of a pixel in the new frame is computed using statistical background model and thresholded to label it as foreground or not. Some morphological operations are applied to remove noise and to close holes in the foreground regions.

In [4], for a color image, if the luminance of an incoming pixel is within the luminance range of the codeword and the dot product of the input RGB with the average value ρ_{RGB} of the codeword is less than a predefined value, the pixel is considered as a background pixel otherwise it is considered as a foreground pixel. For an infrared image, the ratio of pixel value p_T with the maximum value T_{hi} of the codeword (p_T/T_{hi}) and the ratio of is p_T with the minimum value T_{low} of the codeword (p_T/T_{low}) are calculated and these ratios are compared against some predefined thresholds to find foreground pixels.

2.1.4 Fusion of Infrared and Visible Images

In some studies, fusion of infrared and visual information is proposed. Some perform fusion in data level and some others in decision level.

In [1], contours are extracted within selected ROIs in either domain and these are combined into single fused contour image. Fused contours are then closed and completed to form silhouette regions. Input and background gradient information within detected ROIs are evaluated to form Contour Saliency Map (CSM) which shows the reliability degree of that pixel belonging to the boundary of a foreground object. CSM is computed for all ROIs in both thermal and visible domains. After thinning and thresholding operations, binary contour fragments which correspond to the same image region in both thermal and visible domain are fused by applying union operation. Any gaps are connected and completed via an A* search algorithm (described in [26], [27]) before applying the flood-fill operation for creating silhouettes. In the final stage high level processing, temporal filtering, is used to eliminate sporadic detections and confidence value is assigned to each silhouette. Each resulting silhouette in either domain is weighted with a contrast value which represents how distinct that region is from the background model. The ratio of maximum input-background intensity difference within the silhouette region to the intensity range of the background image in both domains is calculated and it gives the confidence value. To further improve detection results, temporal median filter is applied to blobs to eliminate sporadic detections.

Fusion of the infrared and visible domain is done in background modeling in [2] by storing N frames for each band L, U, V and infrared. Single foreground mask is extracted from the foreground detection application which is described in Section 2.1.3.

In [4], fusion of the infrared and visible domain is also in background modeling step where a pixel is assigned as foreground if that pixel is not part of the background model for both domains.

2.2 Algorithms Which Use Infrared or Visible Image

Haritaoglu, *et. al.* [8] present a real time visual surveillance system, W^4, which detects and tracks multiple people and monitors their activities in outdoor environment. It works with a monocular gray-scale camera or an infrared camera.

Bimodal background modeling is used for the statistical background modeling. During the training period, for each pixel, the values of the minimum intensity, the maximum intensity and the maximum intensity difference between consecutive frames are found to model the background. While constructing initial background model, moving foreground pixels are eliminated in two steps. In the first step, a median filter is applied typically 20-40 seconds to each pixel. In the second step, stationary pixels are found by using median and standard deviation of the pixels and only those stationary pixels are taken for the background model. Background model is updated by two methods: a pixel-based update and an object based update. The pixel base update model deals with illumination changes. The object based update deals with physical changes.

Background pixel parameters are compared with incoming pixel intensity and it is decided whether the incoming pixel is foreground or not. The intensity differences between incoming pixel and the corresponding maximum and minimum background pixel are calculated. Incoming pixel is classified as foreground or background pixel by comparing these differences with the weighted maximum intensity difference between consecutive frames of background pixel. Region-based noise cleaning, morphological operations and binary connected component analysis are applied to the extracted foreground regions.

2.3 Algorithms Which Use Only Infrared Image

Zhang, *et. al.* [9] examine the methods which are used for detecting humans in visible spectrum and try to determine if these methods can be applicable for infrared

spectrum. Two feature classes, Edgelets and Histogram of Oriented Gradient (HOG) [10] and two classification models AdaBoost and SVM cascade are extended to infrared images. The proposed method is not constructed based on the reliable model of the background that can be learned. Human detection is treated as a general object classification problem. Two types of local features Edgelets and HOG are transformed into a feature space. To represent an object globally usually comes with the problem of the need for a large number of local features. Selection procedure should be applied to decrease computation cost. After the features have been selected, all the training samples of the object and the background are represented in this feature space. By using these two types of local features Edgelets and HOG, classification is made via AdaBoost cascade classifier and cascade of SVM classifier. In training part, three feature-learner combinations are evaluated: Edgelet based AdaBoost cascade, Edgelet based poly-kernel SVM cascade and HOG based poly-kernel cascade.

Dai, *et. al* [11] present a layered representation for infrared image and demonstrate its effectiveness in pedestrian detection and tracking. IR images are decomposed into background (still objects) and foreground (moving objects) by applying Expectation-Maximization (EM) algorithm. An image is represented by the summation of inverse of mask layer times background layer, foreground layer times mask layer and noise layer. Mask layer includes moving object information and noise layer is represented as a Gaussian distribution from the empirical analysis. Phase correlation method is used to register K infrared images for initial estimation of background. At each iteration, mask layer is updated by thresholding difference of current image with background layer. The alignment results are purified by eliminating foreground pixels. Background layer is updated via adaptively average operation of K registered images. If the difference between current background model and previous one is smaller then a predefined value, iteration will stop. Foreground layer is extracted after finding the background and mask layer.

2.4 Algorithms Which Use Only Visible Image

Zhou and Hoang [12] present a robust real time system which is capable of detecting and tracking the human for video surveillance. This system can also be used in varying environments. Running average method is used to model the background. Background model is updated via an updating rate to deal with gradual light changes. A modified version of background subtraction is used for foreground detection. Some noises caused by motion of camera, shaking of tree are aimed to be eliminated with this modified version. Foreground mask image is constructed by using two threshold values which are applied to the result of background subtraction. The result of the shadow detection module is also used in the construction of foreground mask image.

Hussein, *et. al.* [13] present a real time system for human detection, tracking and verification by using a color camera which is installed on a freely moving platform such as a vehicle or a robot. It is emphasized that system design and implementation are focused rather than algorithmic issue. In [13], before the foreground detection, an image registration algorithm which is described in [14] is applied. It recovers affine motion between a pair of image to align the current frame with a preceding frame and with a succeeding frame. To find foreground regions, the current frame is subtracted from the preceding frame and succeeding frame. Binary image is constructed by thresholding subtracted image. Binary images show locations of foreground regions in the subtracted images. To find foreground regions in current frame, AND operation is applied between two binary images.

In [29], a real-time computer vision and machine learning system is presented to model and recognize human behaviors for visual surveillance. An eigenspace model is used to detect moving objects by using sample images as feature vectors. The dimension of the constructed eigenspace is reduced by applying Principal Component Analysis (PCA). It is aimed to keep K eigenvectors which should represent only the static parts of the scene. Current frame is projected onto the space

spanned by K eigenvectors and the reconstructed frame is obtained. By thresholding the difference between the current frame and the projected frame, foreground regions are extracted.

Salient (interesting e.g, a person) motion detection is performed in [30] by combining temporal difference imaging and a temporal filtered motion field for real-time video surveillance in complex environments. In five steps, the salient moving objects are detected: (1) the temporal differences of consecutive frames are calculated to get region of change; (2) frame to frame optical flow is computed by using Lucas-Kanada method; (3) the temporal filter is applied to the region of changes (found in step one), with the assumption of salient moving objects move in a consistent direction in a period time on X-component or Y-component; (4) the pixels are considered as seed pixels if they move unceasingly in the same direction for the X-component and Y-component of optical flow; (5) salient moving objects are detected by combining the temporal difference imaging, temporal filtered motion and region information.

2.5 Algorithms for Shadow Detection

In [20], shadow detection is performed via comparing the current pixel chrominance and brightness value with the corresponding background pixel values. The computational color model expressed in [23] is used. In this model, a chromaticity line passing through the origin is formed by using the background R, G and B values (mean values) of each pixel location. The distortion of chromaticity line of the current pixel values to the corresponding background model line is calculated for that pixel. Two distortion measurements are calculated: Brightness and chromaticity distortion. The brightness distortion α measures how close the current pixel value to the expected chromaticity line is. The orthogonal distance from the current chromaticity line to the background chromaticity line is defined as the color distortion CD_i. A pixel is considered as a shadow pixel if the brightness distortion α and the chromaticity distortion CD_i .is within some threshold values.

In [2], shadow detection is found by calculating the decrease in brightness and the chromaticity for each pixel. Only mean values of L, U and V bands of the background model are used for these purposes. In order a pixel to be accepted as a potential shadow pixel, some conditions should be satisfied. Detected foreground regions that overlap with the potential shadow regions is computed. If the ratio of shadow region to the overlapped foreground region is within some threshold values, this region is considered as a final shadow region.

CHAPTER 3

APPLIED METHODS

In this chapter, each block of the algorithm is presented one by one. The proposed algorithm requires registered image streams, hence the first step is synchronization in time and space of infrared and visible image pairs of our dataset. In the next step, the various background models are implemented. Each model is described with their own updating parts. The foreground detection for each model is also explained in this chapter. Some of the shadow detection algorithms are presented to remove shadow regions from the detected foreground regions of visible domain. Using the resulting foreground mask, corresponding regions of infrared image is extracted. In the resulting foreground regions, connected components are detected as object candidates. Finally, a snake is fit to each connected component so that the boundaries of the objects are extracted. This snake algorithm is presented at the end of this chapter.

3.1 Image Registration

An external synchronization clock is available neither for our infrared nor for our visible camera. Thus, before registering the images in space, synchronization in time must be completed to get correspondence for the image pairs. For this purpose; evident cues which exist in both domains are chosen manually and frame difference between infrared and visible image sequences is calculated. Figure 3-1 shows an

infrared image which has the frame number 1463 and corresponding visible image pair which has the frame number 1400.

Figure 3-1 Infrared and Visible Image at Frame Number 1463 and 1400 Respectively

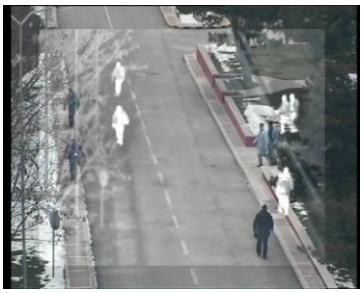

Figure 3-2 Addition of Original Images of Infrared and Color Domain

If the resulting images are used without registration, the results do not give desired outputs. Figure 3-2 shows addition of the infrared and visible image pairs. Spatial registration task is started by finding common field of view manually from the image pairs. After that, the regions which are not seen in both domains are cut out. Sizes of the images in both domains are made similar by up sampling or down sampling via bilinear interpolation. Translation transformation is also applied to the visible image to match it with the corresponding infrared image. After get correspondence for image pairs in space, registration parameters are fixed to use them for all scenes. Figure 3-3 shows registered infrared and visible image. Figure

3-4 shows addition of these registered image pairs. This algorithm is applied to every corresponding image pair in video streams. By using these registered infrared and visible images, two video files are created separately that is a video which includes only registered infrared images and a video which includes only corresponding registered visible images. These registered video files are used in the experiments.

For the other recorded scenarios, just finding frame difference between infrared and visible video streams is enough to register these two streams automatically (because the parameters which are used in registration in space are fixed) by using above registering algorithm for this experimental setup.

Figure 3-3 Registered Infrared and Visible Image

Figure 3-4 Addition of Registered Images of Infrared and Color Domain

3.2 Background Modeling

3.2.1 Single Gaussian Model: Infrared, Color Intensity, Color Channels Separately

In [1], Single Gaussian method is applied at each pixel to model the background. N frames are captured form both infrared and visible domains to construct proper mean/variance background models. Median images I_{med} of both domains are found from the N thermal and visible images. By using the median image, the weight of each pixel is calculated to minimize the effect of the outliers. The weights are computed from a Gaussian distribution centered at $I_{med}(x, y)$

$$w_i(x, y) = \exp\left(\frac{\left(I_i(x, y) - I_{med}(x, y)\right)^2}{-2\hat{\sigma}^2} \right) \tag{3-1}$$

$I_i(x, y)$ values which are far from the median $I_{med}(x, y)$ (outliers) has smaller contribution. $\hat{\sigma}$ represents the standard deviation and it is taken as 5. The statistical background model of each pixel in infrared and intensity component of visible image is constructed by computing weighted mean (3-2) and variance (3-3). For the color channels component of visible image, mean (3-4) and covariance (3-5) are calculated without weights.

$$\mu(x, y) = \frac{\sum_{i=1}^{N} w_i(x, y) \cdot I_i(x, y)}{\sum_{i=1}^{N} w_i(x, y)} \tag{3-2}$$

$$\sigma^2(x, y) = \frac{\sum_{i=1}^{N} w_i(x, y) \cdot (I_i(x, y) - \mu(x, y))^2}{\frac{N-1}{N} \cdot \sum_{i=1}^{N} w_i(x, y)} \tag{3-3}$$

$$\mu(x,y) = \frac{1}{N}\sum_{i=1}^{N} I_i(x,y) \tag{3-4}$$

$$C(x,y) = \frac{1}{N}\sum_{i=1}^{N} (X-u)(X-u)^T \tag{3-5}$$

For longer sequences background model can be updated by using update factor ρ as follows:

$$\mu_t(x,y) = (1-\rho)\cdot\mu_{t-1}(x,y) + \rho\cdot I_t(x,y) \tag{3-6}$$

$$\sigma_t^2(x,y) = (1-\rho)\cdot\sigma_{t-1}^2 + \rho\cdot(I_t(x,y)-\mu_t(x,y))^T \times (I_t(x,y)-\mu_t(x,y)) \tag{3-7}$$

Update factor ρ parameter is chosen different for updating mean and variance of the pixel.

In Figure 3-5, the results of mean images of each infrared, color intensity and color channels domain are shown. These images are taken from frame 300 of sequence1 of OTCBVS dataset. Although mean images of color intensity and color channels contain two transparent people silhouettes, mean image of infrared contains no people silhouettes. One of the people (close to building) stays almost first 150 frames in front of the building and the other one walks along the road up during the frame 300. This situation causes transparent people silhouettes in background model of color domain.

Figure 3-5 Mean Images of Infrared, Color Intensity and Color Channels of Single Gaussian Background Method

3.2.2 Single Gaussian Model: Infrared and Color Intensity as One Vector

In this model, infrared and color intensity are used as one vector to model the background with Single Gaussian method.

$$X = \begin{bmatrix} C_{Int} & IR \end{bmatrix} \tag{3-8}$$

Each pixel is expressed as (3-8). C_{Int} and IR represent the color intensity and infrared components of each pixel respectively. Mean and covariance of this vector is calculated using equations (3-4) and (3-5) without weights. Update procedure is performed similar to the procedure that is expressed in Section 3.2.1 (equations (3-6) and (3-7)).

3.2.3 Single Gaussian Model: Infrared and Color Channels as One Vector

In this model, infrared and color channels are used as one vector to model the background with Single Gaussian method.

$$X = \begin{bmatrix} R & G & B & IR \end{bmatrix} \tag{3-9}$$

Each pixel is expressed as (3-9). R, G, B and IR represent the red, green, blue and infrared components of each pixel respectively. Mean and covariance of this vector is calculated using equations in (3-4) and (3-5) without weights. Update procedure is performed similar to the procedure that is expressed in Section 3.2.1 (equations (3-6) and (3-7)).

3.2.4 Single Gaussian Model: Infrared, Color Intensity and Color Channels as One Vector

In this model, infrared, color intensity and color channels are used as one vector to model the background with Single Gaussian method.

$$X = \begin{bmatrix} R & G & B & C_{Int} & IR \end{bmatrix} \tag{3-10}$$

Each pixel is expressed as (3-10). R, G, B, C_{Int} and IR represent the red, green, blue, color intensity and infrared components of each pixel respectively. Mean and covariance of this vector is calculated using equations in (3-4) and (3-5) without weights. Update procedure is performed similar to the procedure that is expressed in Section 3.2.1 (equations (3-6) and (3-7)).

3.2.5 Non-Parametric Model

In [2], non-parametric background model described in [3] is taken the origin of the background model. The non-parametric model stores N frames for each band L, U, V and infrared. RGB bands are converted to LUV bands to get less correlation between channels such that background model becomes more valid. For each band and for each pixel, consecutive image pair differences $|x_i - x_{i+1}|$ are calculated. Median q of these differences is calculated. Variance of each band σ^2 is found as:

$$\sigma^2 = \frac{q}{0.68\sqrt{2}} \tag{3-11}$$

LUV (also known as CIELUV) is a color space adopted by CIE (International Commission on Illumination). The CIE has defined a system that classifies color according to the HVS, the human visual system. LUV color space is nearly linear with visual perception, or at least as close as any color space is expected to sensibility get and the conversions are reversible. It is device independent but not very intuitive to use.

Conversion of R, G, B to CIE XYZ:

$$\begin{bmatrix} X \\ Y \\ Z \end{bmatrix} = \begin{bmatrix} 0.412453 & 0.357580 & 0.180423 \\ 0.212671 & 0.715160 & 0.072169 \\ 0.019334 & 0.119193 & 0.950227 \end{bmatrix} \begin{bmatrix} R \\ G \\ B \end{bmatrix} \tag{3-12}$$

Conversion CIE XYZ to CIE LUV:

$$\begin{aligned} L &= 116 * Y^{1/3} - 16 \qquad for \quad Y > 0.008856 \\ L &= 903.3 * Y \qquad\quad for \quad Y \le 0.008856 \end{aligned} \tag{3-13}$$

$$\begin{aligned} u' &= 4 * X / (\mathrm{X} + 15 * \mathrm{Y} + 3 * \mathrm{Z}) \\ \mathrm{v}' &= 9 * \mathrm{Y} / (\mathrm{X} + 15 * \mathrm{Y} + 3 * \mathrm{Z}) \end{aligned} \tag{3-14}$$

$$\begin{aligned} u &= 13 * L * (u' - u_n) \qquad where \quad u_n = 0.19793943 \\ \mathrm{v} &= 13 * L * (v' - v_n) \qquad where \quad v_n = 0.46831096 \end{aligned} \tag{3-15}$$

On output $0 \le L \le 100$, $-134 \le u \le 220$, $-140 \le v \le 122$. The values are then converted to the destination data type:

$$\begin{aligned} L &= L * 255/100 \\ u &= (u + 134) * 255/354 \\ v &= (v + 140) * 255/256 \end{aligned} \tag{3-16}$$

Conversion of CIE XYZ to R, G, B:

$$\begin{bmatrix} R \\ G \\ B \end{bmatrix} = \begin{bmatrix} 3.240479 & -1.53715 & -0.498535 \\ -0.969256 & 1.875991 & 0.041556 \\ 0.055648 & -0.204043 & 1.057311 \end{bmatrix} \begin{bmatrix} X \\ Y \\ Z \end{bmatrix} \quad (3\text{-}17)$$

Before modelling background, anisotropic diffusion and rough pedestrian detection are performed.

Anisotropic Diffusion:

Infrared images are processed to deal with noises. Due to the nature of the infrared radiation, hot objects including the device itself emit non-significant amounts of radiation at this spectrum. Hence infrared images contain high noise. To reduce these noises, anisotropic diffusion is applied to each infrared image.

The following algorithm is applied iteratively to the smoothed version of the infrared image I until convergence for anisotropic diffusion (by observing the results of anisotropic diffusion, five iterations are enough to get the convergence). An isotropic Gaussian kernel is applied for smoothing:

1. Gradient magnitude is calculated for the smoothed image.

$$M = |\nabla I| \quad (3\text{-}18)$$

2. Coefficients C are calculated.

$$C = \frac{1}{M+1} \quad (3\text{-}19)$$

3. Each pixel in I is multiplied with its corresponding coefficient in C .

4. I is set with the given equation (3-20). $F(X)$ is obtained by replacing each value in X , with the sum of eight neighbors of the value and the value itself.

$$I = F(I)/F(C) \quad (3\text{-}20)$$

Infrared frame 5 (in Figure 3-6) of sequence1 of OTCBVS dataset is used to demonstrate anisotropic diffusion. The results of the first and the fifth iterations of anisotropic diffusion operation are shown in Figure 3-7.

Figure 3-6 Infrared Frame 5 of Sequence1 of OTCBVS Dataset

Figure 3-7 First and Fifth Iteration of Anisotropic Diffusion Respectively

If a 5x5 Gaussian kernel is applied five times to the same infrared image given in Figure 3-6, the result will be so blurred as shown in Figure 3-8. As can be seen from Figure 3-7, anisotropic diffusion operation preserves edges while smoothing internal regions.

Figure 3-8 Fifth Iteration of Gaussian Filter

Rough Pedestrian Detection:

Before initializing background model, a rough pedestrian detection is made in the infrared image by using size, aspect ratio and thermal features. It is aimed to not to miss any pedestrians, so that their pixels are not put into the background model. Regarding the observation of an infrared image histogram, a dominant Gaussian distribution is contained in the histogram which represents environment temperature (essentially noise). Interest of objects is assumed to have brighter pixels and lie far outside this distribution. An importance score function (3-21) is generated for each brightness value by using the histogram. Each pixel is replaced with the importance value of its brightness.

$$u(x) = \left(\frac{1}{\frac{h(x)}{\max(h)} + 1} \right)^n \tag{3-21}$$

Where x represents pixel brightness value, $h(x)$ is the histogram of infrared image and n is a parameter which decreases importance value of noises. n is taken as 10. After replacing each pixel by its importance value, two threshold values T_L and T_U are applied for segmentation of hysteresis. All pixels which are below T_L are discarded. From the remaining connected components only those regions which contain at least one pixel which is greater than T_U are taken into consideration for

valid regions. From these regions, non-pedestrians are eliminated if any of the following statements are true:

1. $s_r < S_{\min} \quad or \quad s_r > S_{\max}$
2. $b_r < 1 \quad or \quad b_r > 5$
3. $(a_r - m)/\sigma \leq 2.5$
4. $(m_r - m)/\sigma \leq 4$

Where s_r represents its pixel area, b_r is the height to width ratio of its bounding box using original infrared image (not the importance image), a_r represent its average brightness, and m_r is the maximum brightness. m and σ are the mean and standard deviation of the pixel brightness in the infrared image. $S_{\min}$ and $S_{\max}$ are set empirically regarding the expected pedestrian size. Namely $S_{\min}$ is set to one-quarter of the size of the smallest expected pedestrian and $S_{\max}$ is set to slightly greater than the largest expected pedestrian size. The output of this rough pedestrian detection is a binary mask $P(x, y)$. All the parameters for detecting pedestrians are chosen empirically, and it is aimed to not miss any pedestrians so that their pixels are not put into the background model.The same infrared image in Figure 3-6 is taken to show some results of the rough pedestrian detection algorithm. Non-pedestrian elimination step and the meanings of colours are shown in Figure 3-9. Elimination order is the same as in the table. If the region is failed from applied condition, it is filled with corresponding colour and no more comparison is done for this particular region.

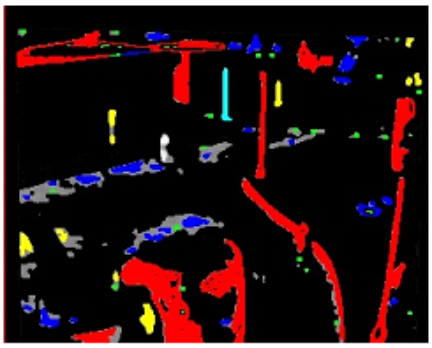

	Color	Meaning
1	Red	$s_r > S_{max}$
2	Green	$s_r < S_{max}$
3	Blue	$b_r < 1.2$
4	Turquoise	$b_r > 5$
5	Yellow	$(a_r - m)/\sigma \leq 1.8$

Figure 3-9 Non-Pedestrian Detection and Meaning of Colors

In Figure 3-10 output of the rough pedestrian detection is shown. Morphological dilation operation is applied to the result with 5x5 rectangle structural element and it is shown also in the same figure.

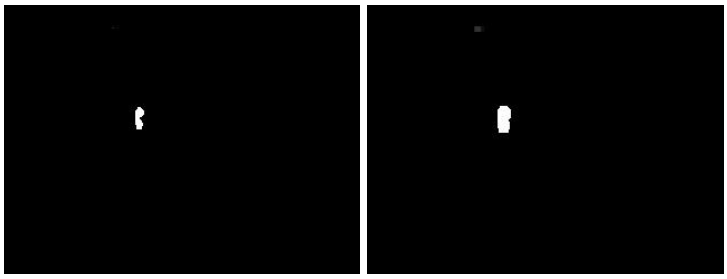

Figure 3-10 Output of Rough Pedestrian Detection and Dilation Operation

One of the people (in Figure 3-6) is detected, but the other one is eliminated. Because the upper part of the body, which has a temperature value close to the pavement, is connected with a part of the pavement. This connected component exceeds the specified maximum area limit.

Background Updating:

Background modeling is updated for the purpose of dealing with gradual changes like day to night changes. The objects are also placed to the background, in following cases: If the objects remain enough time in the scene and if the objects

are decided as foreground by mistake such as caused by rapid changes. This update procedure should also be capable of updating quickly in the presence of ghost objects or sudden illumination changes. Background modeling process has been performed continuously to deal gradual changes. Background modeling B, is updated by the following rules:

1. if $\Gamma(x, y) \geq 1$, update $B(x, y)$, where Γ is explained below
2. otherwise, if $B(x, y)$ =? (unknown), update $B(x, y)$ only if $P(x, y) = 0$
3. otherwise, if this pixel is classified as shadow, it is not updated
4. otherwise, update this pixel if it has been detected as background

If the Background model has already N samples, the new coming pixel is updated by oldest sample, if the model is less than N samples, it is added to the sample set. The variances of each band are also periodically updated.

Likelihood image $\Gamma(x, y)$ finds cues and takes the pixel to the corresponding background model. These cues are time, size, edge magnitude and thermal brightness. If an object spends enough long time in the scene, it should be treated as background. Normally, tinny areas appearing in the foreground regions are caused by detection errors. Edges give cues about the foreground region. These cues tell if the background is a ghost or not. Thermal cue is based on the assumption that the colder objects are more likely to be part of background model. Each pixel location of $\Gamma(x, y)$, which is detected as a foreground pixel, is updated as follows:

$$\Gamma_{x,y,t} = \Gamma_{x,y,t-1} + C_T + f_{T_s,\sigma_s}(s_r) + f_{T_e,\sigma_e}(e_r) + f_{T_b,\sigma_b}(b) \tag{3-22}$$

$$f_{T,\sigma}(x) = C\left(1 - \frac{1}{1 + e^{\frac{-(x-T)}{\sigma}}}\right) \tag{3-23}$$

$$e_r = \frac{1}{|\delta r|}\sum_{i \varepsilon \delta r}(|\nabla I(i)| - |\nabla B(i)|) \qquad (3\text{-}24)$$

where, s_r is the size of foreground region which includes the pixel (x, y), b is the maximum thermal brightness in a $7x7$ window around the pixel (x, y) within the same foreground region area, C_T is time constant to determine how fast static objects will be part of the background model, C is constant to control the function value. Gradient values corresponding to the boundaries of the detected foreground regions and the background regions (δr is the set of these points) are calculated. Differences of these values are accumulated to get e_r value. This approach is based on [22]. The function of $f_{T,\sigma}(x)$ is a sigmoid function which has center point at T and whose transition width is controlled by σ. Parameters of equation (3-22), are chosen empirically.

The value of the background likelihood of the pixel which is greater than 1 ($\Gamma(x, y) \geq 1$), is shown as an image in Figure 3-11 (from frame 300 of sequence1 of OTCBVS dataset). This image is constructed by using each cue given in equation (3-22). During the 300 frames, one of the people (close to building) stands almost first 150 frames on front of the building and the other one walks along the road. The standing person pixels are starting to be taken into the background frames because of time cue C_T. The other person causes ghost regions behind. For these situations, edge cues give more information. Because there exist normally no human in the current image so value of the term $f_{T_e,\sigma_e}(e_r)$ in equation (3-22) increases. Tinny areas, which are detected as a foreground, are updated because of size cue $f_{T_s,\sigma_s}(s_r)$. The colder objects which are detected as foreground, are also updated because of thermal cue $f_{T_b,\sigma_b}(b)$.

Figure 3-11 Likelihood Image of the Non-Parametric Method

3.2.6 Non-Parametric Model: Infrared and Color Separately

The same procedure as the one described in Section 3.2.5 is applied in this method. Anisotropic diffusion and the rough pedestrian detection module are performed on the infrared image. Update procedure is also the same, as the one described in Section 3.2.5.

3.2.7 Mixture of K Gaussian Model

In [19] each pixel in the background model is modeled by a mixture of *K* Gaussian distributions. The probability of a pixel's having a value of x_N at time N can be written as:

$$p(x_N) = \sum_{k=1}^{K} w_k \eta(x_N; \Theta_k) \tag{3-25}$$

$$\eta(x; \Theta_k) = \eta(x; \mu_k, \Sigma_k) = \frac{1}{(2\pi)^{\frac{D}{2}} |\Sigma_k|^{\frac{1}{2}}} e^{-\frac{1}{2}(x-\mu_k)^T \Sigma_k^{-1} (x-\mu_k)} \tag{3-26}$$

where w_k is the weight parameter, μ_k is the mean and $\Sigma_k = \sigma_k^2 \mathrm{I}$ is the covariance of the k[th] component. R, G and B components are assumed to be independent. The initial weights of the *K* distributions at time N are adjusted as:

$$w_k^{N+1} = (1-\alpha) w_k^N + \alpha \hat{\rho}(w_k \mid x_{N+1}) \tag{3-27}$$

where α is the learning rate and $\hat{\rho}(w_k \mid x_{N+1})$ is 1 for the first matched Gaussian component and 0 for the remaining part. w_k^N represents weight parameter at time N of the k[th] component. The K Gaussian distributions are ordered by the value of w_k / σ_k and the first *B* distributions are used for the background modeling.

$$B = \arg\min_b \left(\sum_{k=1}^{b} w_k > T \right) \tag{3-28}$$

where *T* represents the threshold for the minimum portion of the background model. Every new pixel value x_t is checked against existing *K* Gaussian distributions until a match is found. A match is defined as a pixel value within 2.5 standard deviations of a distribution. If there is no match, the mean of the least probable distribution is replaced with the current value and initially high variance and low prior weights are assigned to this distribution. If there is a match to one of the components, first matched model component will be updated as follows:

$$\mu_k^{N+1} = (1-\rho) u_k^N + \rho x_{N+1} \tag{3-29}$$

$$\sigma_{k,N+1}^2 = (1-\rho)\sigma_{k,N}^2 + \rho (x_{N+1} - u_k^{N+1})^T (x_{N+1} - u_k^{N+1}) \tag{3-30}$$

where the second learning rate, ρ is

$$\rho = \alpha \eta(x_{N+1} \mid \mu_k^N, \sigma_k^N) \tag{3-31}$$

μ_k^N and σ_k^N represent mean and variance values at time *N* of the k[th] component.

In [20], an improved version of [19] is explained. Initial estimation of Gaussian mixture model is made up with static update equations given below:

$$w_k^{N+1} = w_k^N + \frac{1}{N+1} \left(\hat{\rho}(w_k \mid x_{N+1}) - w_k^N \right) \tag{3-32}$$

$$\mu_k^{N+1} = \mu_k^N + \frac{\hat{\rho}(w_k \mid x_{N+1})}{\sum_{i=1}^{N+1} \hat{\rho}(w_k \mid x_i)} (x_{N+1} - \mu_k^N) \tag{3-33}$$

$$\sum_k^{N+1} = \sum_k^N + \frac{\hat{\rho}(w_k \mid x_{N+1})}{\sum_{i=1}^{N+1} \hat{\rho}(w_k \mid x_i)} \left((x_{N+1} - \mu_k^N)(x_{N+1} - \mu_k^N)^T - \sum_k^N \right) \tag{3-34}$$

when the first L samples are processed, L-recent window version equations are used as given below:

$$w_k^{N+1} = w_k^N + \frac{1}{L} \left(\hat{\rho}(w_k \mid x_{N+1}) - w_k^N \right) \tag{3-35}$$

$$\mu_k^{N+1} = \mu_k^N + \frac{1}{L} \left(\frac{\hat{\rho}(w_k \mid x_{N+1}) x_{N+1}}{w_k^{N+1}} - \mu_k^N \right) \tag{3-36}$$

$$\sum_k^{N+1} = \sum_k^N + \frac{1}{L} \left(\frac{\hat{\rho}(w_k \mid x_{N+1})(x_{N+1} - \mu_k^N)(x_{N+1} - \mu_k^N)^T}{w_k^{N+1}} - \sum_k^N \right) \tag{3-37}$$

In Figure 3-12, the results of mean images of each infrared, color intensity and color channels domain are shown. These images are taken from frame 300 of sequence1 of OTCBVS dataset. Sudden illumination changes occur during the sequence in visible domain. This situation affects the model of the background in that domain. The effect of these sudden illumination changes can be seen on the background model, in front of the building (Figure 3-12).

Figure 3-12 Mean Images of Infrared, Color Intensity and Color Channels of Mixture of Gaussian Background Method

3.3 Foreground Detection

3.3.1 Foreground Detection Based on Single Gaussian Background Model

In [1], the squared Mahalanobis distance is used for foreground detection. For the infrared and intensity component of visible image, foreground detection is made by equation (3-38). For the color channels component of visible image, it is made by (3-39)

$$D(x,y)=\begin{cases}1 & \dfrac{(I(x,y)-\mu(x,y))^2}{\sigma(x,y)^2} \;\rangle\; Z^2 \\ 0 & otherwise\end{cases} \tag{3-38}$$

$$D(x,y)=\begin{cases}1 & (x-\mu)^T C^{-1}(x-\mu) \;\rangle\; Z^2 \\ 0 & otherwise\end{cases} \tag{3-39}$$

Where Z represents the threshold value. Each threshold value, for either of the infrared, the color intensity and the color channels, is set empirically. Especially in infrared domain, it is aimed to detect whole regions of the people if it is possible.

For the Single Gaussian background models which are explained in Sections 3.2.2, 3.2.3 and 3.2.4, the foreground regions are extracted with the same equation given in (3-39).

To demonstrate the results of foreground detection based on the Single Gaussian background model, frame 803 of sequence4 of the OTCBVS dataset is chosen. The current images of infrared, color intensity and color channels are given in Figure 3-13.

Figure 3-13 Current Infrared, Color Intensity and Color Channels Image (Frame 803 of Sequence4 of the OTCBVS Dataset)

The results of foreground regions (for the images given in Figure 3-13) of the Single Gaussian method, which is described in Section 3.2.1 is shown in Figure 3-14. The color domain contains highly spurious foreground regions, if it is not masked by infrared foreground. Some of the spurious foreground regions (for example rectangle regions) are detected because of compression of row data. Foreground regions of color intensity and color channels which are masked by infrared foreground are shown in Figure 3-15. Spurious foreground regions of the color domain are mostly removed by masking them with foreground regions of infrared domain.

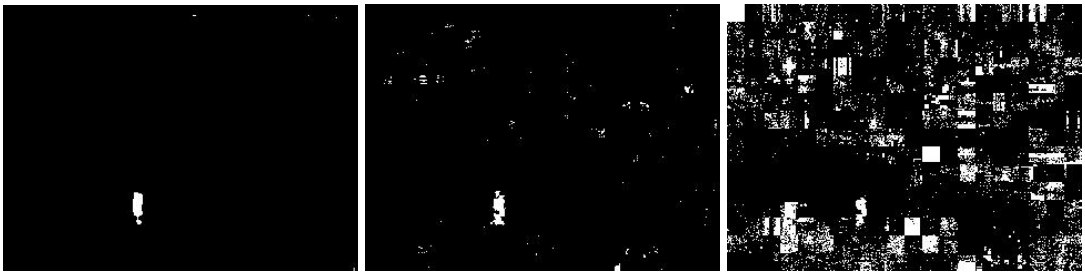

Figure 3-14 Foreground Regions of Infrared, Color Intensity and Color Channels (without Masked by Infrared Foreground)

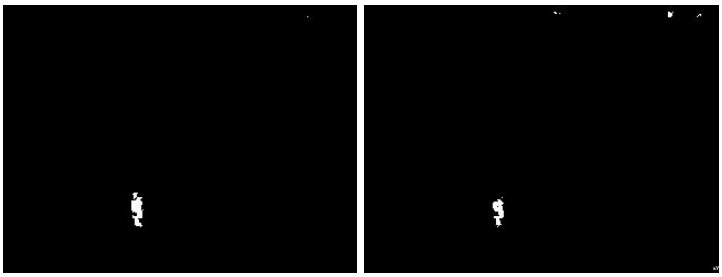

Figure 3-15 Foreground Regions of Color Intensity and Color Channels (with Masked by Infrared Foreground)

In Figure 3-16, foreground regions of Single Gaussian methods which are modelled by combinations of bands as one vector (described in Section 3.2.2, 3.2.3 and 3.2.4) are shown. The leftmost image shows the foreground regions of the Single Gaussian model which is constructed by infrared and color intensity modelled as one vector (described in Section 3.2.2). The middle image shows the foreground regions of which infrared and color channels are represented as one vector (described in Section 3.2.3) to model the background. The rightmost image shows the foreground regions of the model which is constructed by representing each infrared, color intensity and color channels domain as one vector (described in Section 3.2.4). As can be seen from the images, many spurious foreground regions are detected for all combinations. Some of the spurious foreground regions especially in rightmost image (for example rectangle regions) are detected because of compression of row

data. Trying to model each domain as one vector causes the model to be more sensitive to noises.

Figure 3-16 Foreground Regions of Single Gaussian Methods (Combination of Bands as One Vector)

3.3.2 Foreground Detection Based on Non-Parametric Background Model

In [2], for a new pixel the probability that it came from the background distribution is calculated as below:

$$\Pr(x_t) = \frac{1}{N}\sum_{i=1}^{N}\prod_{j=1}^{d}\frac{1}{\sqrt{2\pi\sigma_j^2}}e^{-\frac{1}{2}\frac{(x_{tj}-x_{ij})^2}{\sigma_j^2}} \tag{3-40}$$

where N and d represent the number of stored frames and used channels respectively. d is taken 4 for this model that is L, U, V and infrared domains. σ_j^2 represents the variance of corresponding channels.

If the $\Pr(x_t)$ of a new pixel is lower than a threshold, it is taken as a foreground pixel. If the pixel has zero samples due to binary mask $P(x, y)$ from the rough pedestrian detection module, it is taken as a foreground pixel as well.

To demonstrate the results of foreground detection based on the Non-Parametric background model, the same figure (Figure 3-13) is chosen. In Figure 3-17, the results of the foreground regions of Non-Parametric model, which is described in Section 3.2.5, is shown. Equation (3-40) is used to detect foreground regions. The foreground region of non-parametric model does not contain so many foreground regions. In addition, human regions of the foreground are close to manually segmented foreground.

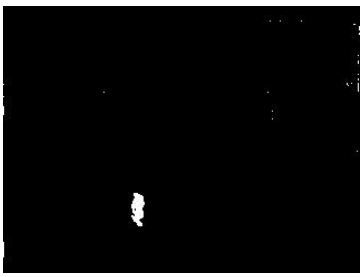

Figure 3-17 Foreground Regions of Non-Parametric Method

In the non-parametric model, for which infrared and color domains are modeled separately (described in Section 3.2.6), the foreground regions in the infrared domain are extracted by using equation (3-40) (d parameter is taken 1 for only infrared band). The foreground regions found in the color domain are extracted from foreground regions found in the infrared domain by using the same equation (3-40) (d parameter is taken 3 for L, U and V bands).

To show results of foreground detections of each band, the same figure (Figure 3-13) is chosen. In Figure 3-18, the left image shows the foreground regions of infrared and the right image shows foreground regions of LUV image without using infrared foreground as a mask image. In Figure 3-19, the foreground region of LUV image is shown with using infrared foreground as a mask image. By applying infrared foreground as a mask image, the spurious regions are mostly removed from the foreground region of LUV.

Figure 3-18 Foreground Regions of Infrared and LUV (without Masked by Infrared Foreground)

Figure 3-19 Foreground Regions of LUV (with Masked by Infrared Foreground)

3.3.3 Foreground Detection Based on Mixture of Gaussian Background Model

In [19], by considering the equation (3-28), a pixel is classified as a foreground pixel, if it is more than 2.5 standard deviations away from any of the *B* distributions. The threshold *T* is a measure of the minimum portion of the background model. If it is chosen too high desired foreground regions cannot be detected. Especially in infrared domain, it is aimed to detect whole regions of the person.

The results of foreground regions (for the images given in Figure 3-13) of the Mixture of Gaussian method, which is described in Section 3.2.7, are shown in Figure 3-20. The color domain contains also shadow regions, if it is not masked by infrared foreground. Foreground regions of color intensity and color channels which

are masked by infrared foreground are shown in Figure 3-21. Shadow regions of the foreground regions of the color domains are mostly removed by masking them with foreground regions of infrared domain.

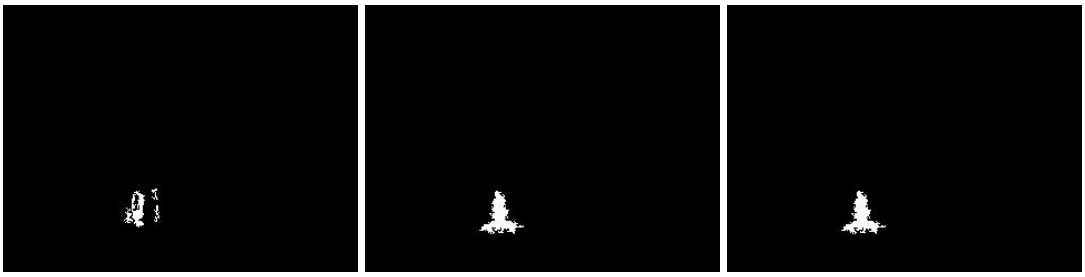

Figure 3-20 Foreground Regions of Infrared, Color Intensity and Color Channels (without Masked by Infrared Foreground)

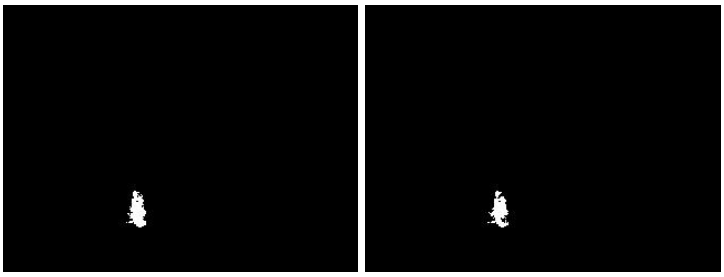

Figure 3-21 Foreground Regions of Color Intensity and Color Channels (with Masked by Infrared Foreground)

3.3.4 Shadow Detection

3.3.4.1 Method-1 for Shadow Detection

If a pixel will be considered a shadow pixel, difference between ratios of the normalized components of each channel of the current pixel and the background model should be lower than a threshold value.

$$\left| \frac{R_c,\ G_c,\ B_c}{R_c + G_c + B_c} - \frac{R_b,\ G_b,\ B_b}{R_b + G_b + B_b} \right| < Th \qquad (3\text{-}41)$$

where subscript c demonstrates the current pixel and b demonstrates the background model of that pixel. If the above equation is hold true for each color channel component of the pixel, it is considered as a shadow pixel.

To demonstrate the results of shadow detection algorithm, frame 319 is taken from the sequence2 of the OTCBVS dataset which is shown in Figure 3-22.

Figure 3-22 Frame 319 of Sequence2 of the OTCBVS Dataset for Shadow Detection

The result of method-1 for shadow detection is given in Figure 3-23. Left image shows the result of the condition equation (3-41) and the right image shows the masked image with the foreground region of color image. Desired shadow regions could not be extracted by applying the equation (3-41). It is almost impossible to eliminate shadows from the foreground regions of color image by this method. So, it is not used in our algorithm.

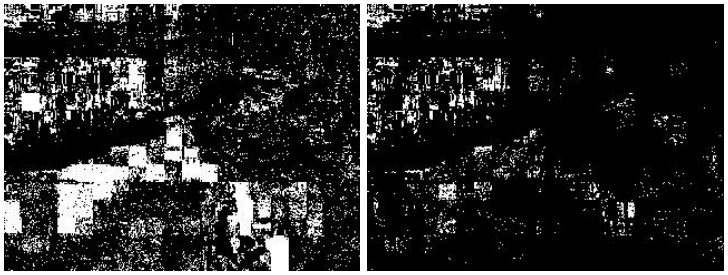

Figure 3-23 Shadow Detection Results for Method-1, Originally Shadow Image and Final Shadow Image After Masked with Foreground Region of Color Image

3.3.4.2 Method-2 for Shadow Detection

In [20], shadow detection is performed via comparing the current pixel chrominance and brightness value with the corresponding background pixel values. The computational color model expressed in [23] is used. In this model, a chromaticity line passing through the origin is formed by using the background R, G and B values (mean values) of each pixel location. The distortion of chromaticity line of the current pixel values to the corresponding background model line is calculated for that pixel. Two distortion measurements are calculated: Brightness and chromaticity distortion. The brightness distortion α measures how close the current pixel value to the expected chromaticity line is. It is a scalar value and is calculated by minimizing the equation given below:

$$\Phi(\alpha_i) = (I_i - \alpha_i E_i)^2 \tag{3-42}$$

where E_i is the expected color of the background model.

The orthogonal distance from the current chromaticity line to the background chromaticity line is defined as the color distortion CD_i and calculated as given below:

$$CD_i = \left\| I_i - \alpha_i E_i \right\| \tag{3-43}$$

After some derivations, brightness distortion and color distortion are calculated by the equations given below;

$$\alpha_i = \frac{\left(I_R(i)\mu_R(i) + I_G(i)\mu_G(i) + I_B(i)\mu_B(i)\right)}{\left((\mu_R(i))^2 + (\mu_G(i))^2 + (\mu_B(i))^2\right)} \tag{3-44}$$

$$CD_i = \sqrt{(I_R(i) - \alpha_i\mu_R(i))^2 + (I_G(i) - \alpha_i\mu_G(i))^2 + (I_B(i) - \alpha_i\mu_B(i))^2} \tag{3-45}$$

A pixel is considered as a shadow pixel if brightness distortion α is within 2.5 standard deviation and the condition of $\tau < CD_i < 1$ is true for chromaticity distortion CD_i.

The same figure (Figure 3-22) is used to demonstrate the result of method-2. In Figure 3-24, the left image shows the original shadow regions where conditions of brightness α and chromaticity distortion CDi are hold true. The right image shows the masked image with foreground regions of color image. This method is not used in our algorithm, because the shadow regions could not be differentiated from the foreground regions of color image, as it can be seen in Figure 3-24.

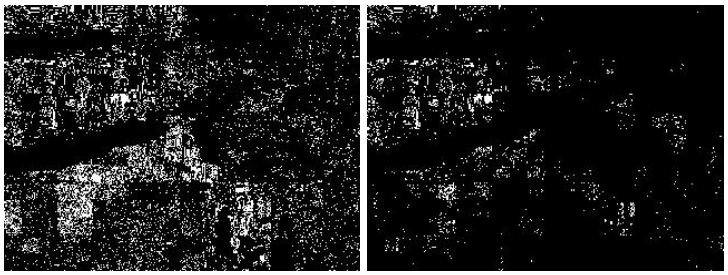

Figure 3-24 Shadow Detection Results for Method-2, Originally Shadow Image and Final Shadow Image After Masked with Foreground Region of Color Image

3.3.4.3 Method-3 for Shadow Detection

In [2], shadow detection is found by calculating the decrease in brightness and the chromaticity for each pixel. Only mean values of L, U and V bands of the background model are used for these purposes. In order a pixel p to be accepted as a shadow pixel, all the conditions below should be satisfied:

1. $0.8 \le C_L \le 0.98$, where $C_L = p_L / B_L$

2. $C_{UV} \le 20$, where $C_{UV} = \sqrt{(B_U - p_u)^2 + (B_V - p_V)^2}$

Where C_L is the change of luminance, C_{UV} is the change of chrominance, B_L, B_U and B_V are the average background values of each band. These pixels are considered as potential shadow pixels. Detected foreground regions that overlapped with the potential shadow regions is computed and the ratio of:

$$\Theta = \left| S \right| \Big/ \left| F \right| \tag{3-46}$$

is calculated. Where, $|S|$ is the area of the shadow and $|F|$ is the area of the foreground regions. Final shadow regions are found by the condition: $\alpha \le \Theta \le \beta$. α and β parameters limit the shadow region area with the corresponding overlapped foreground. α and β parameters are set such that any of the person regions do not considered as shadow regions.

The same figure (Figure 3-22) is used to demonstrate the result of method-3. In Figure 3-25, left image shows possible shadow regions before the application of condition equation (3-46) and the right image shows the result of shadow detection after applying the equation. As it can be seen in Figure 3-25, almost whole shadow regions are detected as possible shadow regions. Final shadow regions are extracted

from these possible shadow regions. This method is used in our algorithm to remove shadow regions from the foreground regions of color domain.

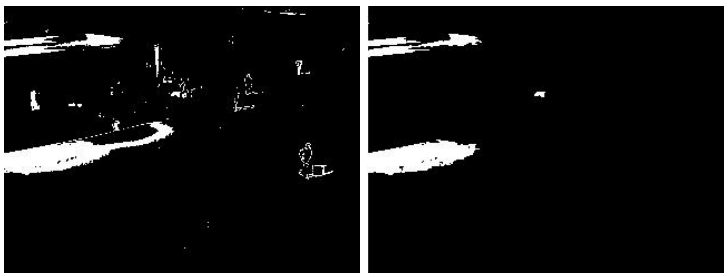

Figure 3-25 Shadow Detection Results for Method-3, Possible Shadow Image and Final Shadow Image

3.3.5 Fusion of Infrared and Visible Domains

For the background models, (described in Section 3.2.1, 3.2.6 and 3.2.7) where the infrared and color domains are modeled separately, the fusion of the infrared and visible domain is performed as explained below:

Pixel-wise OR operation is applied between the foreground regions of masked color intensity and color channels. From these regions, detected shadows regions are removed. After shadow elimination from the foreground regions of color domain, pixel-wise OR operation is applied between these regions and the foreground regions of the infrared. The resulting foreground regions are used as a mask in the application of the snake algorithm.

To demonstrate the results of fusion of infrared and visible domains based on the Single Gaussian (SG), Mixture of Gaussian (MOG) and Non-Parametric (Non-Param) background models (described in Section 3.2.1, 3.2.6 and 3.2.7), frame 665 is taken from the sequence3 of the OTCBVS dataset which is shown in Figure 3-26. As it can be seen from Figure 3-27, Figure 3-28 and Figure 3-29 some regions of the people cannot be detected, furthermore the person regions are divided into at

least two parts in infrared domain. After the addition of the color foreground, these regions are almost completed as seen in the rightmost image of each figure.

Figure 3-26 Current Infrared, Color Intensity and Color Channels Image (Frame 665 of Sequence3 of the OTCBVS Dataset)

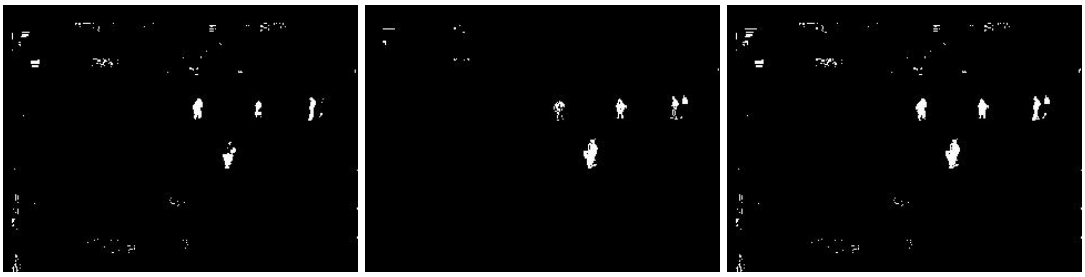

Figure 3-27 Foreground Region of Infrared, Foreground Region of Color and Resulting Final Foreground (Based on SG Background Model)

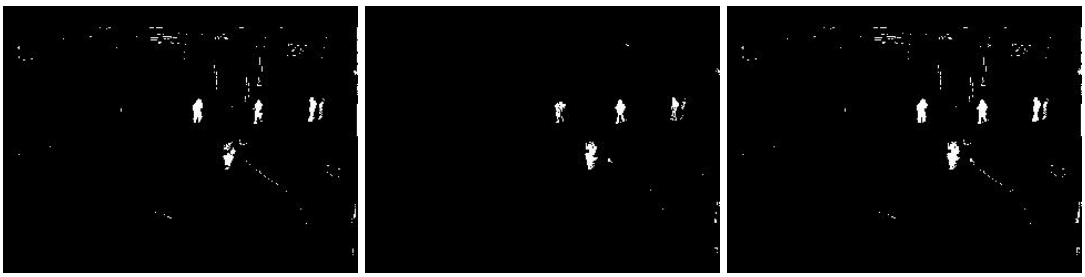

Figure 3-28 Foreground Region of Infrared, Foreground Region of Color and Resulting Final Foreground (Based on Non-Param Background Model)

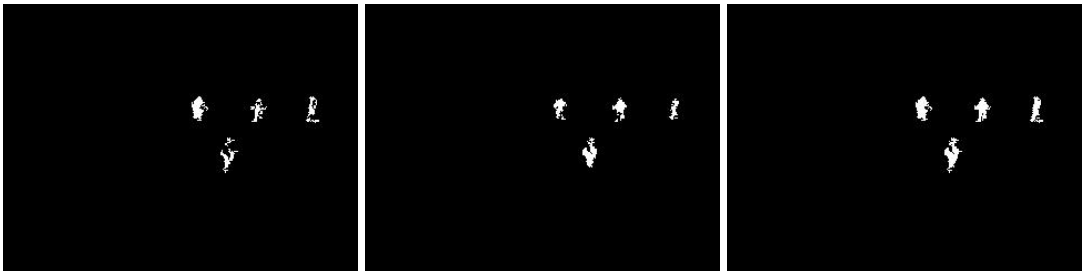

Figure 3-29 Foreground Region of Infrared, Foreground Region of Color and Resulting Final Foreground (Based on MOG Background Model)

For the background models, (described in Section 3.2.2, 3.2.3, 3.2.4, 3.2.5) fusion of the infrared and color domain is performed in background model. For the Single Gaussian methods, a pixel is represented as a vector which contains each domain and only one foreground region is extracted by applying the equation (3-39). For the Non-Parametric method, N frames are stored for each band and only one foreground region is extracted by applying the equation (3-40). Finally shadow regions are removed from these foreground regions and it is used as a mask for the application of snake algorithm.

Frame 240 is taken from the sequence4 of the OTCBVS dataset which is shown in Figure 3-30 to demonstrate the results. In Figure 3-31, the leftmost image shows the final foreground regions of the Single Gaussian model which is constructed by infrared and color intensity modelled as one vector (described in Section 3.2.2). The next image shows the final foreground regions of which infrared and color channels domains are represented as one vector (described in Section 3.2.3) to model the background. The next image shows the final foreground regions of the model which is constructed by representing each infrared, color intensity and color channels domain as one vector (described in Section 3.2.4). Rightmost image shows the final foreground regions of Non-Parametric background model (described in Section 3.2.5).

As it can be seen from the Figure 3-31, final foreground region, which is based on Non-Parametric background model, does not contain so many spurious and it is so

close to the manually segmented human region. Representing the combinations of each band as one vector does not give desired results.

Figure 3-30 Current Infrared, Color Intensity and Color Channels Image (Frame 240 of Sequence4 of the OTCBVS Dataset)

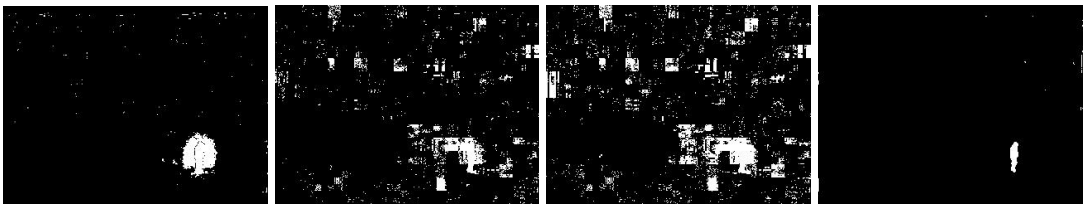

Figure 3-31 Final Foreground Regions (Combination of Bands as One Vector of Single Gaussian and Non-Parametric Background Model)

3.4 Application of Snake Algorithm

The main goal of active contour models or snakes is to detect objects in a given image, by evaluating a curve. In [21] Chan and Vese proposed a model which can detect objects whose boundaries are not necessarily defined by gradient. It is based on Mumford-Shah segmentation techniques [28] and the level set method. The model is trying to separate the image into regions based on intensities. Starting with a curve whose position can be anywhere in the image, the curve moves toward its interior normal and stops on the boundary of the object. The main problem is the minimization of energy based-segmentation.

To explain the main idea in a simple way, the equation (3-47) can be considered:

$$F_1(C)+F_2(C) = \int_{inside(C)} |u_0(x,y) - c_1|^2 dxdy + \int_{outside(C)} |u_0(x,y) - c_2|^2 dxdy \quad (3\text{-}47)$$

where C is the curve which will be evolved, $u_0(x,y)$ is the given image and it is assumed that two regions exist in the image which has approximately constant intensities. c_1 and c_2 are the average intensity values of the inside and outside of the C. It can be seen that the boundary of the object C_0 will minimize the (3-47)

After adding some regularizing terms to (3-47), the energy function becomes:

$$\begin{aligned} F(c_1,c_2,C) &= \mu \cdot Length(C) + \nu \cdot Area(inside(C)) + \\ &\lambda_1 \int_{inside(C)} |u_0(x,y) - c_1|^2 dxdy + \lambda_2 \int_{outside(C)} |u_0(x,y) - c_2|^2 dxdy \end{aligned} \quad (3\text{-}48)$$

Where $\mu \geq 0$, $\nu = 0$, $\lambda_1 = \lambda_2 = 1$ and the problem becomes of minimization of $F(c_1,c_2,C)$ with respect to c_1, c_2 and C. The model is solved by level set formulation. The contour $C \subset \Omega$ is represented by the zero level set of a Lipschitz function $\phi : \Omega \to \Re$ such that

$$\begin{cases} C = \{(x,y) \ \varepsilon \ \Omega : \phi(x,y) = 0\}, \\ inside(C) = \{(x,y) \ \varepsilon \ \Omega : \phi(x,y) > 0\}, \\ outside(C) = \{(x,y) \ \varepsilon \ \Omega : \phi(x,y) < 0\}, \end{cases}$$

Introducing the Heaviside function *H*, and the one-dimensional Dirac measure δ_0, the terms in the energy function of *F* can be expressed as:

$$\begin{aligned} L\{\phi = 0\} &= \int_\Omega \delta(\phi(x,y)) |\nabla \phi(x,y)| dxdy \\ A\{\phi \geq 0\} &= \int_\Omega H(\phi(x,y)) dxdy \end{aligned} \quad (3\text{-}49)$$

The intensity terms:

$$\begin{aligned}\int_{\phi>0}\left|u_0(x,y)-c_1\right|^2 dxdy &= \int_{\Omega}\left|u_0(x,y)-c_1\right|^2 H(\phi(x,y))dxdy \\ \int_{\phi<0}\left|u_0(x,y)-c_2\right|^2 dxdy &= \int_{\Omega}\left|u_0(x,y)-c_2\right|^2 (1-H(\phi(x,y)))dxdy\end{aligned} \tag{3-50}$$

The average intensities c_1 and c_2 can be calculated as:

$$\begin{aligned}c_1(\phi) &= \frac{\int_{\Omega} u_0(x,y)H(\phi(x,y))dxdy}{\int_{\Omega} H(\phi(x,y))dxdy} \\ c_2(\phi) &= \frac{\int_{\Omega} u_0(x,y)(1-H(\phi(x,y)))dxdy}{\int_{\Omega} (1-H(\phi(x,y)))dxdy}\end{aligned} \tag{3-51}$$

Minimizing *F* function with respect to ϕ is done by Euler-Lagrange equation while keeping c_1 and c_2 constant:

$$\frac{\partial\phi}{\partial t} = \delta(\phi)\left[\mu\kappa(\phi)\left|\nabla\phi\right| - \nu - \lambda_1(u_0-c_1)^2 + \lambda_2(u_0-c_2)^2\right] \tag{3-52}$$

where the curvature κ can be expressed as:

$$\begin{aligned}\kappa(\phi) &= -div\left(\frac{\nabla\phi}{|\nabla\phi|}\right) \\ \kappa(\phi) &= \frac{\phi_{xx}\phi_y^2 - 2\phi_{xy}\phi_x\phi_y + \phi_{yy}\phi_x^2}{(\phi_x^2+\phi_y^2)^{3/2}}\end{aligned} \tag{3-53}$$

The basic algorithm:

1. Initialization n and contour ϕ (any shape can be the initialization shape)
2. Increase *n* by 1

3. Compute the average intensities c_1 and c_2 of the image pixels inside and outside (3-51)

4. Evolve the level set function (3-52)

5. Repeat the steps 2, 3 and 4 until the solution is stationary or *n* exceeds the limit of iteration

The algorithm given in [24] is tried to be implemented for this purpose. This algorithm is applied to each connected component of the foreground image extracted from the thermal channel. To get more precise results, the area and the center of each connected component are computed and used for the initialization of the snake. The shape of the contour is chosen as a circular. The radius of the circle and the iteration number of the algorithm is changed according to the area of the connected component.

To demonstrate the results of application of snake algorithm, frame 319 is taken from the sequence2 of the OTCBVS dataset which is shown in Figure 3-32. Because of the halo effect around the people is weaker for this OTCBVS dataset and the background temperature is so close to the human temperature, in the snake algorithm, contour can not surround the boundary of the human objects as it can be seen in Figure 3-33. In our database the halo effects that surround the people are more evident than in OTCBVS dataset and contour could surround the boundary of the human objects more precisely. The results of the application of snake algorithm are also given in Section 4.4.

Figure 3-32 Current Infrared, Color Intensity and Color Channels Image (Frame 319 of Sequence2 of the OTCBVS Dataset)

Figure 3-33 Foreground Region of Infrared, Resulting Final Foreground Region and Application of Snake Algorithm

CHAPTER 4

EXPERIMENTAL RESULTS

In this study, various background models are implemented to get foreground regions and proposed snake algorithm is applied to the final foreground regions in order to detect people in two different databases. One of them is the "OSU Color-Thermal Dataset" in OTCBVS benchmark [25] and the other one is constructed by us. Results are demonstrated and compared against manually segmented human regions. Our results are also compared with a previous study [1] (described in Section 2.1).

"OSU Color-Thermal Dataset" contains six challenging thermal/color video sequences. They are recorded from two different locations, at different times of the day and with different camera gain and level settings. Our dataset also contains six challenging thermal/color video sequences. Three different places are used for recording at different times of the day and recorded with different camera gain and level settings.

4.1 Experimental Setup

The main parts of the experimental setup are as follows:

i) A box which consists of an infrared and a visible camera: The infrared camera, TU2, is a long wave infrared imaging camera designed for use in the security industry. The infrared detector has the features: 320 x 240

pixels, Uncooled Focal Plane Array, 625 Lines (PAL/CCIR) Compliant. The visible camera, EQ2700, is ¼" day/night camera. The specifications of the EQ2700: PAL signal system, total pixels no. 795 (H) x 596 (V), electronic shutter 1:50~1:10000, 1 Vp-p composite PAL, BNC, S-video mini DIN video output, 27x optical and 10x digital zoom.

ii) Two PAL recorders (Mini-DV) to record each video stream.

iii) An interface box: It is prepared to control the parameters of both infrared and visible camera and also provide links between PAL recorders and cameras. For infrared camera, by using focus switch, far/near focusing is adjusted, by using polarity switch, black/white polarity is chosen, via gain and level button, gain and level tuning is done. For visible camera, parameters can be changed via RS232 connection.

iv) Power supply unit to supply the cameras.

Figure 4-1 shows the components of our experimental setup and one of the experimental setup places.

Figure 4-1 Experimental Setup and Place

Scenarios are recorded into tapes via PAL recorders. Recorded videos are captured by using Microsoft Windows Movie Maker via IEEE1394 port. Captured frames are

saved using digital device format (DV-AVI). Xvid MPEG-4 codec is used to compress saved file to save space in the storage device. The proposed algorithms are applied to these recorded files.

4.2 Background Modelling

Background modelling methods which are described in Section 3.2 are implemented. Some of the results are presented to compare differences of the methods.

In Figure 4-2, the results of mean images of each infrared, color intensity and color channels domain of the Single Gaussian method, which is described in Section 3.2.1, are shown. The results of the Mixture of Gaussian which is described in Section 3.2.7, is also given in Figure 4-3. These images are taken from frame 300 of scene3 of our dataset. One person walks through the road and gets out of the sight of the cameras during the frame 300. The path followed by the person can be seen on the mean image of the color channels based on the Single Gaussian method (in Figure 4-2). Whereas the mean image of the color channels, which is based on the Mixture of Gaussian background model, does not include this path and it is modelled more correctly.

Figure 4-2 Mean Images of Infrared, Color Intensity and Color Channels of Single Gaussian Background Method

Figure 4-3 Mean Images of Infrared, Color Intensity and Color Channels of Mixture Gaussian Background Method

4.3 Foreground Detection

In this part, detected foreground regions for each background model is presented. The foreground detection algorithms are explained in Section 3.3.

To demonstrate the foreground regions for all background modelling methods from our dataset, the current images of infrared, color intensity and color channels which are shown in Figure 4-4, are taken from frame 373 of scene2 of our dataset.

Figure 4-4 Current Infrared, Color Intensity and Color Channels Image (Frame 373 of Scene2 of Our Dataset)

The results of foreground regions (for the images given in Figure 4-4) of the Single Gaussian method, which is described in Section 3.2.1 is shown in Figure 4-5. In our dataset, the halo effects around the people are more evident than OTCBVS dataset.

The color domain contains highly spurious foreground regions, if it is not masked by infrared foreground. Some of the spurious foreground regions (for example rectangle regions) are detected because of compression of row data. Foreground regions of color intensity and color channels which are masked by infrared foreground are shown in Figure 4-7. Spurious regions of the foreground regions of the color domains are mostly removed by masking them with foreground regions of infrared domain.

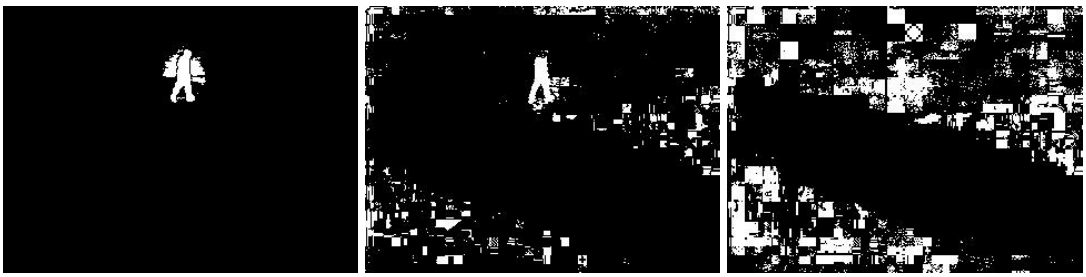

Figure 4-5 Foreground Regions of Infrared, Color Intensity and Color Channels (without Masked by Infrared Foreground) Based on Single Gaussian Background Model

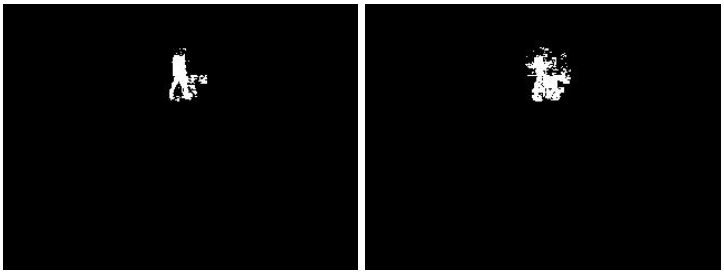

Figure 4-6 Foreground Regions of Color Intensity and Color Channels (with Masked by Infrared Foreground) Based on Single Gaussian Background Model

The results of foreground regions (for the images given in Figure 4-4) of the Mixture of Gaussian method, which is described in Section 3.2.7, are shown in Figure 4-7. The color domain contains spurious foreground regions and also shadow regions. Spurious foreground regions are reduced compared with Single Gaussian

method (Figure 4-7). They are mostly removed by masking them with infrared foreground. The results are shown in Figure 4-8.

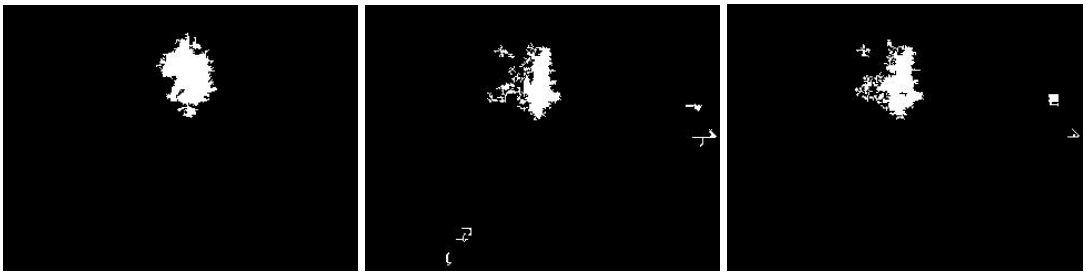

Figure 4-7 Foreground Regions of Infrared, Color Intensity and Color Channels (without Masked by Infrared Foreground) Based on Mixture of Gaussian Background Model

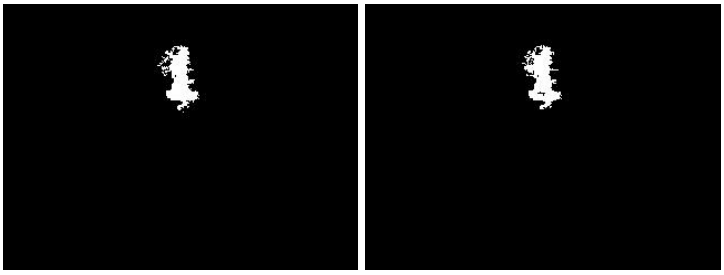

Figure 4-8 Foreground Regions of Color Intensity and Color Channels (with Masked by Infrared Foreground) Based on Mixture of Gaussian Background Model

In Figure 4-9, the results of the foreground regions of Non-Parametric model with IR and L, U, V bands used separately which is described in Section 3.2.6, are shown. Left image shows foreground regions of infrared and the right image shows foreground regions of LUV image without using infrared foreground as a mask image. By applying infrared foreground as a mask image to the foreground regions of LUV image, the spurious regions are mostly removed (see Figure 4-10). Silhouette of the person is more evident for foreground region of color domain in this model compared with Single Gaussian and Mixture of Gaussian background models.

Figure 4-9 Foreground Regions of Infrared and LUV (without Masked by Infrared Foreground) Based on Non-Parametric Method

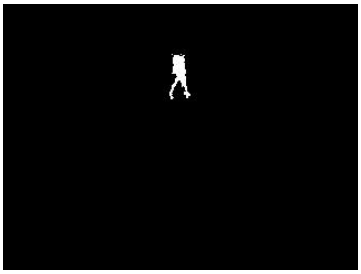

Figure 4-10 Foreground Regions of LUV (with Masked by Infrared Foreground) Based on Non-Parametric Method

In Figure 4-11, the results of the foreground regions of Non-Parametric model which is described in Section 3.2.5, are shown. The foreground region of non-parametric model does not contain so many spurious foreground regions. In addition, human regions of the foreground are close to the manually segmented human regions.

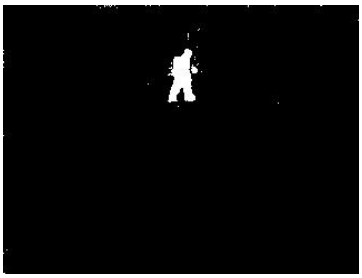

Figure 4-11 Foreground Regions of Non-Parametric Method

In Figure 4-12, foreground regions of Single Gaussian methods which are modelled by combinations of bands as one vector (described in Section 3.2.2, 3.2.3 and 3.2.4) are shown. The leftmost image shows the foreground regions of the Single Gaussian model which is constructed by infrared and color intensity modelled as one vector (described in Section 3.2.2). The middle image shows the foreground regions of which infrared and color channels domains are represented as one vector to model the background (described in Section 3.2.3). The rightmost image shows the foreground regions of the model which is constructed by representing each infrared, color intensity and color channels domain as one vector (described in Section 3.2.4). As can be seen from the images, many spurious regions are detected for all combinations. Some of the spurious foreground regions especially in middle and rightmost image (for example rectangle regions) are detected because of compression of row data.

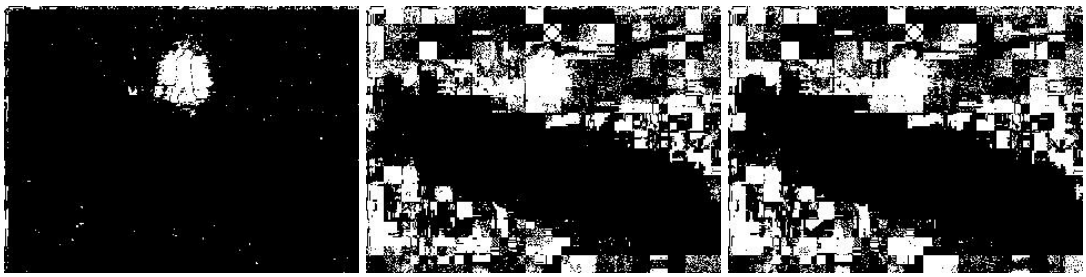

Figure 4-12 Foreground Regions of Single Gaussian Methods (Combination of Bands as One Vector)

4.3.1 Fusion of Infrared and Visible Domain

When the temperature of an object and its surrounding area is closer, detection of the object from thermal image becomes more difficult. In these situations, if the colors of the object and the background are not similar and illumination is available, visual spectrum cameras give more cues that can be used to detect the object. This situation is illustrated in Figure 4-14. The leftmost image shows the foreground detection in infrared domain without the addition of foreground in the visible domain. As can be seen in the image, some regions of the people cannot be detected, furthermore the person regions are divided into at least two parts. The middle image shows the foreground regions of color domain. After the addition of the visible cues, these regions are almost completed as seen in the rightmost image in Figure 4-14. This completion procedure is described in Section 3.3.5. These images are taken from the results of foreground regions based on Single Gaussian background modeling (described in Section 3.2.1) and frame 1721 of scene3 is used from our database.

Figure 4-13 Frame 1712 of Scene3 of Our Dataset for Fusion of Infrared and Visible Domain

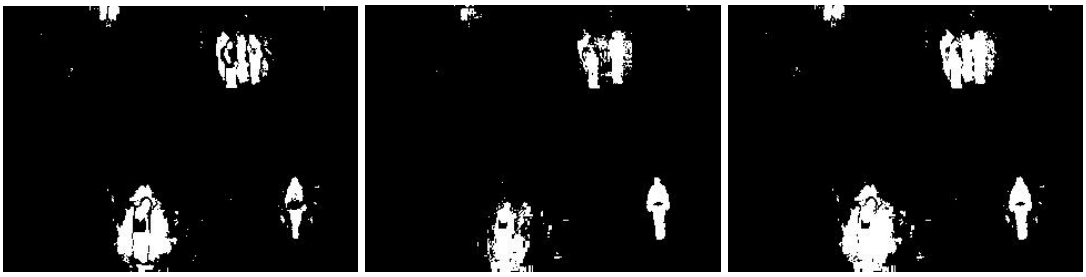

Figure 4-14 Completion of Infrared Foreground Regions, Foreground Region of Infrared, Color Domain and Resulting Final Foreground

4.4 Application of Snake

To demonstrate the results of application of snake algorithm (described in Section 3.4), frame 1400 is taken from the scene4 of our dataset which is shown in Figure 4-15. One of the examples of the application of snake algorithm is illustrated in Figure 4-16. The leftmost image shows the detected foreground regions of the infrared image including the objects (people) and the halo effects around them. The middle image shows the constructed final foreground region. The snake algorithm is applied to each connected component of the image which is formed by masking the infrared image by the constructed foreground mask. The result of the snake algorithm is shown in the rightmost image of Figure 4-16. Here, people are segmented and the boundaries of people are very clear.

Figure 4-15 Frame 1400 of Scene4 of Our Dataset for Fusion of Infrared and Visible Domain

Figure 4-16 Foreground Region of Infrared, Resulting Final Foreground Region and Application of Snake Algorithm

4.5 Performance for the Whole Algorithm

To measure the performance of our algorithm and to compare the results with the results given in [1], the human regions of the 60 image pairs from the "OSU Color-Thermal Dataset" in OTCBVS benchmark (10 frames for each sequence) are manually segmented. All the parameters and threshold values are fixed to present the applicability of the proposed algorithm for various sequences. Different background models are used to demonstrate the affects of background model to the results.

The performance is also presented by Recall (R) (Sensitivity), Precision (P) (Positive Predictive Value) and F-measure values (described in [1]). Recall indicates the ratio of object pixels that the algorithm has found correctly over actually manually segmented region. Precision indicates the ratio of object pixels that the algorithm has found correctly over in fact object regions. F-measure is a harmonic mean of the precision and the recall value.

Let S(A) represents the area of the object pixels that the algorithm has found correctly and let S(B) represents the area of the object pixels that manually segmented.

Recall value is calculated as:

$$\frac{S(A \cap B)}{S(B)} \tag{4-1}$$

Precision value is calculated as:

$$\frac{S(A \cap B)}{S(A)} \tag{4-2}$$

F-measure value is calculated as:

$$F = \frac{2PR}{P + R} \tag{4-3}$$

Especially threshold values for detecting foreground regions are tuned to get best performance from these measurement values and the threshold values are fixed for all sequences before application of the proposed algorithm.

Quantitative results for six sequences are summarized in comparison with [1] in Table 4-1. Different background modeling methods are used to reveal the effect of the results. In the Table 4-1:

SG: the method where each band infrared, color intensity and color channels, is modeled separately as a Single Gaussian (described in Section 3.2.1). The block schema of the algorithm is given in Figure 4-17.

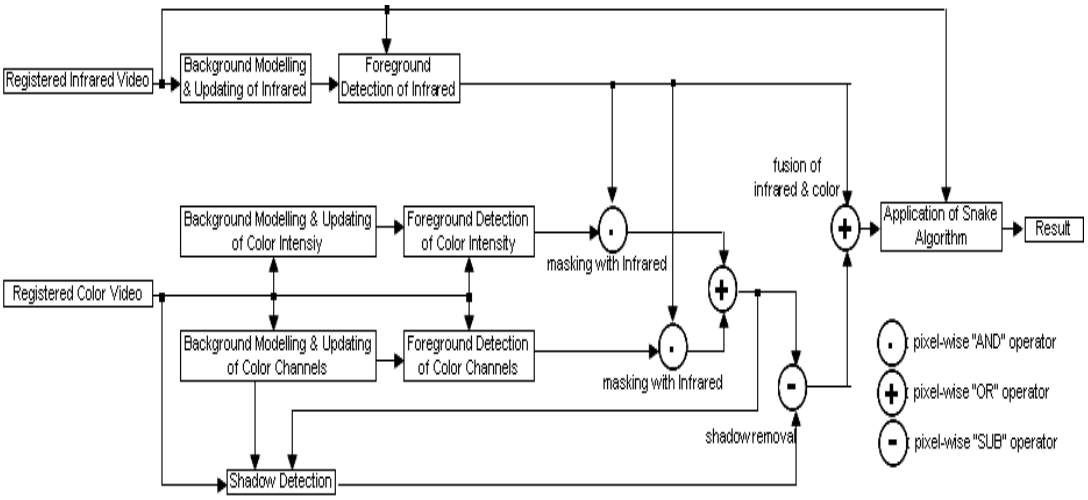

Figure 4-17 The Block Schema of the Algorithm Based on SG and MOG Background Models

MOG: the method where each band, infrared, color intensity and color channels, is modeled separately as a Mixture of Gaussian (described in Section 3.2.7). The block schema of the algorithm is given in Figure 4-17.

Non-Param-1: the method where each band, infrared and color domains, is modeled separately as a Non Parametric (described in Section 3.2.6). The block schema of the algorithm is given in Figure 4-18.

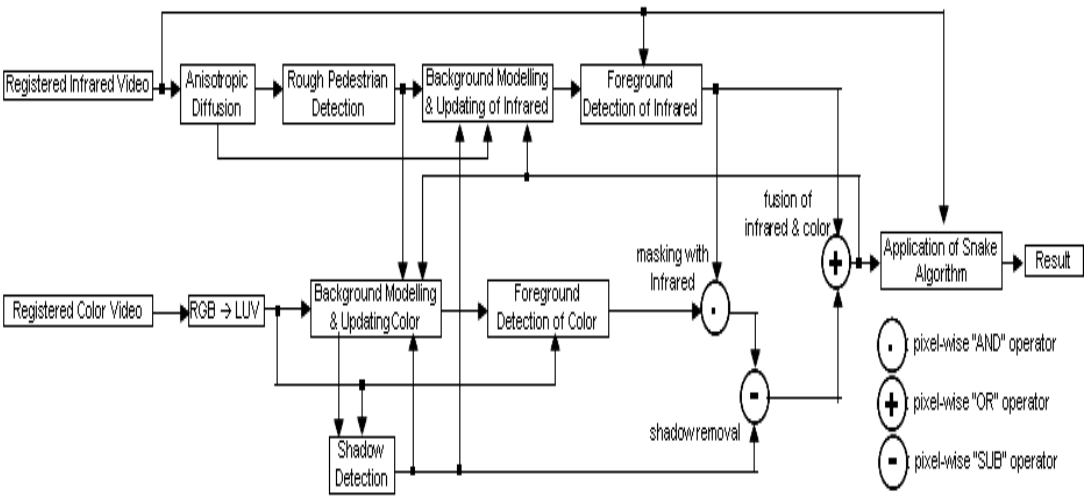

Figure 4-18 The Block Schema of the Algorithm Based on Non-Param-1 Background Model

Non-Param-2: the method where each band is modeled as a Non Parametric in the background model by storing N frames (described in Section 3.2.5). The block schema of the algorithm is given in Figure 4-19.

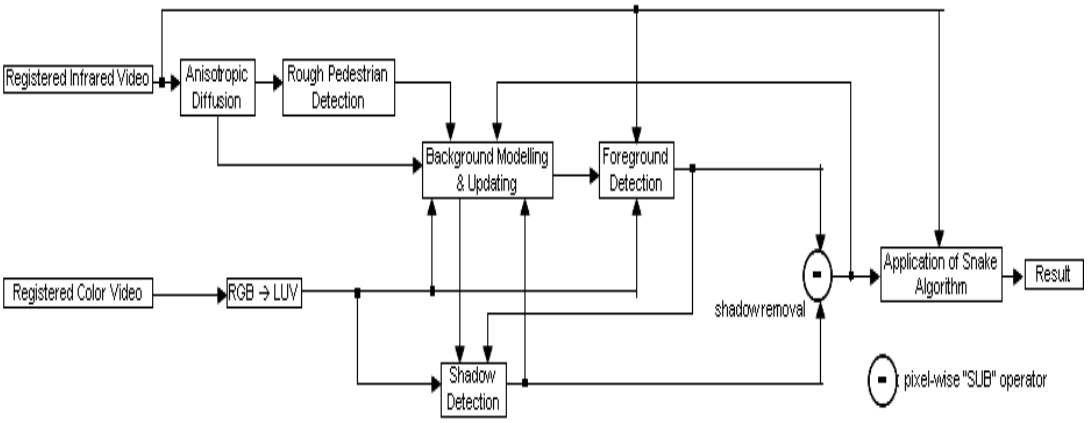

Figure 4-19 . The Block Schema of the Algorithm Based on Non-Param-2 Background Model

In all sequences, for our algorithm, recall values are higher but the precision values are smaller than the ones expressed in [1]. This means that more actual regions are detected. And the main reason of smaller precision is the weakness of the halo

effects surrounding the people in this database. In the snake algorithm, contour can not surround the boundary of the human objects exactly. And also if the temperature of the human object is close to the temperature of the background, contour also includes background objects.

From the comparison of background modeling techniques, the results can be explained as follows:

MOG method has the weakest performance for all quantitative measurement parameters. Especially, the low Precision value shows that extracted foreground regions from the MOG method includes much more spurious regions around the people. Because of the halo effect around the people is weaker for this OTCBVS dataset and the background temperature is so close to the human temperature, in the snake algorithm, contour can not surround the boundary of the human objects and the contour surrounds also these spurious regions. It causes this poor Precision value.

Non-Param-2 method has higher Precision and F-measure values. Detected foreground regions from this model are so close to the manually segmented data, that the contour of the snake algorithm could surround human objects more precisely. The background updating procedure can also be affecting these results. But this updating procedure is more complex and also consumes much more time from other updating procedures described in Section 3.2. Because of the non-existence of infrared foreground mask in this model, the results of this model include some of spurious and shadow regions.

SG and Non-Param1 methods also give promising results for this dataset and have similar quantitative measurements.

Table 4-1 Comparison of Results: Our Algorithm (Based on Kinds of Background Modelling) and Reference [1]

Sequences		SG	MOG	Non Param-1	Non Param-2	In [1]
Seq1	Recall	0.731	0.793	0.786	0.753	0.714
	Precision	0.722	0.564	0.659	0.712	0.914
	F-Measure	0.726	0.659	0.717	0.732	0.802
Seq2	Recall	0.811	0.705	0.786	0.800	0.719
	Precision	0.722	0.658	0.731	0.770	0.874
	F-Measure	0.764	0.680	0.757	0.785	0.789
Seq3	Recall	0.748	0.776	0.753	0.767	0.655
	Precision	0.915	0.822	0.822	0.879	0.905
	F-Measure	0.823	0.799	0.786	0.819	0.760
Seq4	Recall	0.912	0.894	0.834	0.892	0.734
	Precision	0.747	0.660	0.842	0.921	0.955
	F-Measure	0.821	0.760	0.838	0.907	0.830
Seq5	Recall	0.915	0.587	0.873	0.900	0.809
	Precision	0.705	0.612	0.822	0.905	0.957
	F-Measure	0.796	0.599	0.847	0.902	0.877
Seq6	Recall	0.962	0.939	0.922	0.954	0.780
	Precision	0.569	0.412	0.697	0.814	0.931
	F-Measure	0.715	0.573	0.847	0.878	0.851
Overall	Recall	0.846	0.782	0.826	0.844	0.722
	Precision	0.730	0.621	0.762	0.833	0.916
	F-Measure	0.784	0.693	0.793	0.839	0.808

The results from each sequence are visualized below where the first row includes from left to right the tested images of infrared, color intensity, color channels and manually segmented human regions. The second row shows the output of the proposed algorithm. In the second row, leftmost image is based on SG method, the next image is based on MOG method, the next one is based on Non-Param-1 method and the rightmost image is based on Non-Param-2 method.

Figure 4-20 Results from Frame 652 of Sequence1 of OTCBVS Dataset

Figure 4-21 Results from Frame 442 of Sequence2 of OTCBVS Dataset

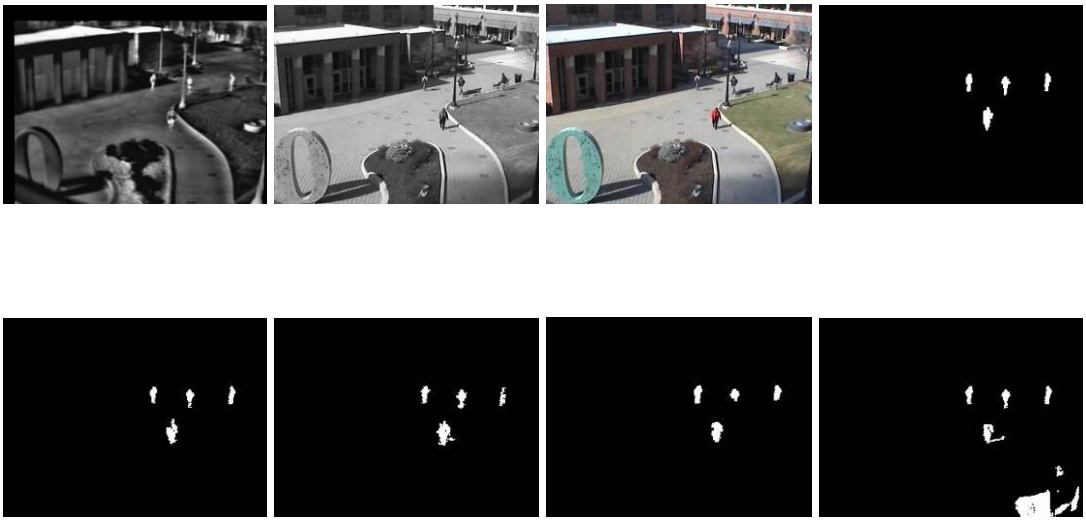

Figure 4-22 Results from Frame 680 of Sequence3 of OTCBVS Dataset

Figure 4-23 Results from Frame 803 of Sequence4 of OTCBVS Dataset

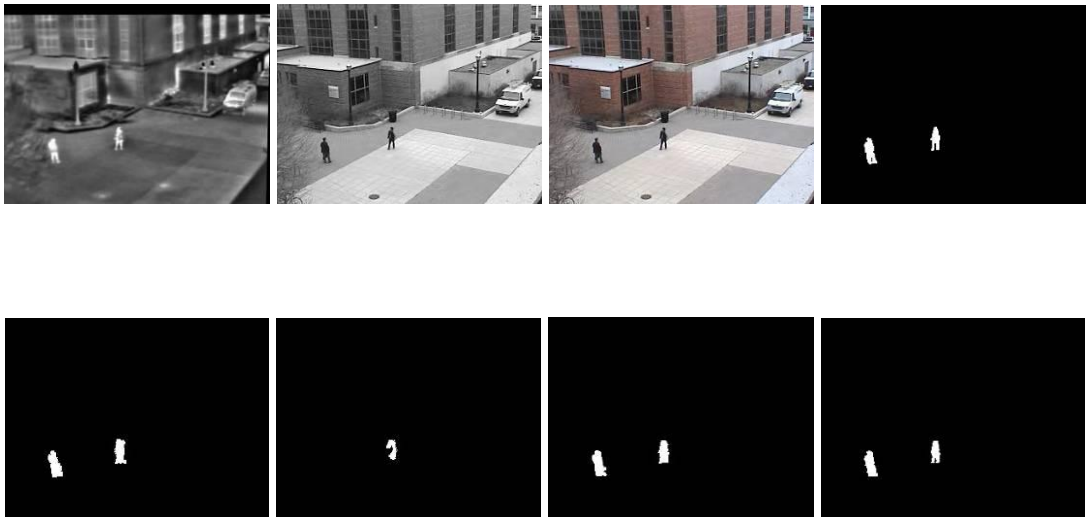

Figure 4-24 Results from Frame 508 of Sequence5 in OTCBVS Dataset

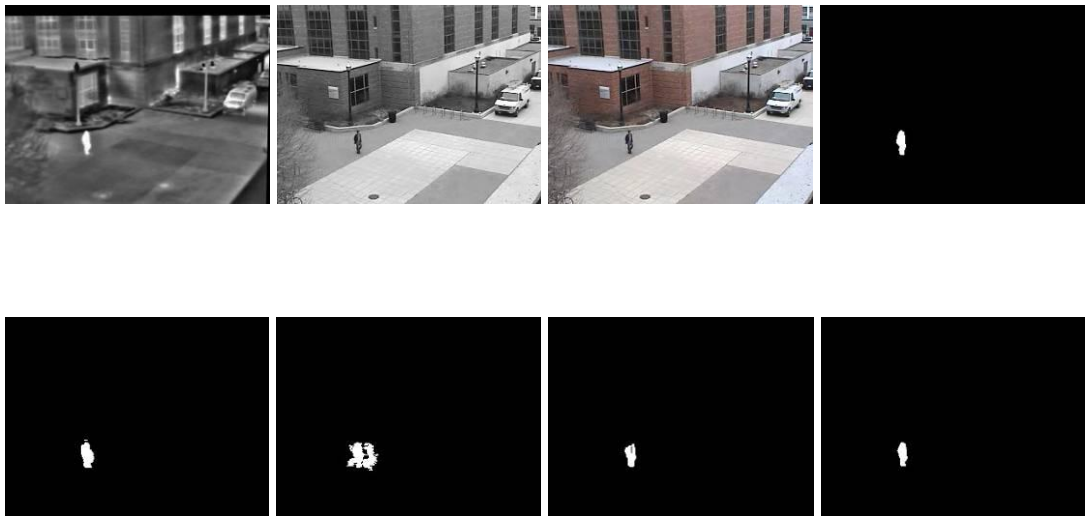

Figure 4-25 Results from Frame 820 of Sequence6 in OTCBVS Dataset

The results of our algorithm when Single Gaussian method is used for background modelling (described in Section 3.2.2, 3.2.3 and 3.2.4) where combinations of each band are represented as one vector, is shown as on a single sequence. The reason of for this is that highly spurious foreground regions are detected when this background modelling is used.

The results are presented in Table 4-2. Where SG-1 stands for a background model where infrared and color intensity domains are expressed as one vector (described in Section 3.2.2). SG-2 stands for a background model where infrared and color channels domains are expressed as one vector (described in Section 3.2.3). SG-3 stands for a background model where infrared and color intensity and color channels domains are expressed as one vector (described in Section 3.2.4). SG-4 stands for a background model where infrared and color channels (L, U and V bands) are expressed as one vector. The block schema of the algorithm is given in Figure 4-26. For the SG-4 model, the color conversion is performed RGB to LUV before processing the color image.

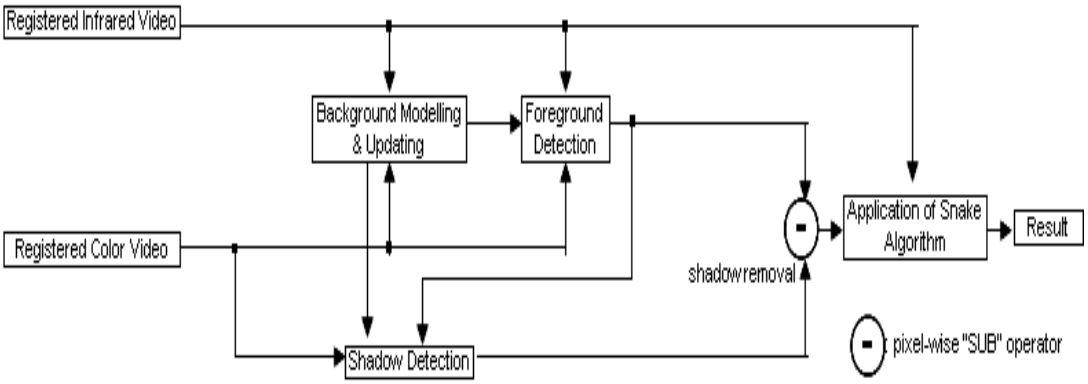

Figure 4-26 The Block Schema of the Algorithm Based on Single Gaussian where Combinations of each band is modelled as One Vector

Although SG-1 has the weakest performance for Precision and F-measure value, it has the maximum Recall value and minimum spurious regions compared to the other two methods. Most spurious regions are detected from the SG3 and this model is the most sensitive model to noises. Foreground regions for all four methods include highly spurious regions around the people. Contour can not surround the boundary of the human objects and it surrounds also these spurious regions. So, it causes this poor Precision value for these methods.

Table 4-2 Results of Our Algorithm Based on Single Gaussian Methods (Combination of Bands as One Vector) and Reference [1]

Sequences		SG-1	SG-2	SG-3	SG-4	In [1]
Seq4	Recall	0.887	0.742	0.779	0.706	0.734
	Precision	0.387	0.573	0.524	0.531	0.955
	F-Measure	0.539	0.647	0.626	0.606	0.830

The results from each sequence are visualized below where the first row includes the tested images of infrared, color intensity, color channels and manual segmented human regions. The second row shows the output of our proposed algorithm. In the second row, leftmost image is based on SG-1 method, the next image is based on SG-2 method, the next image is based on SG-3 and the rightmost image is based on SG-4 method.

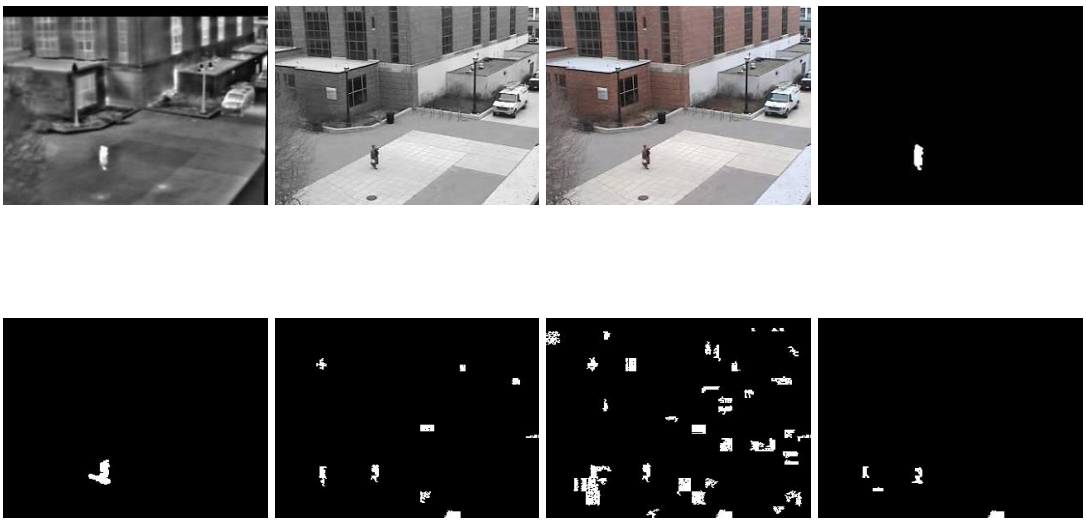

Figure 4-27 Results from Frame 803 of Sequence4 of OTCBVS Dataset

Our database is also used to measure the performance of our proposed algorithm. In our database the halo effects that surround the people are more evident than in OTCBVS dataset. From each sequence, 10 frames are selected and compared with the manually segmented regions. Quantitative results are given in Table 4-3 for our database. All of the parameters and threshold values are fixed to present the applicability of the proposed algorithm for various sequences. Different background models are used to demonstrate the effects of background modelling to the results. In our dataset, the performance of the algorithm is also demonstrated when only infrared domain is used based on Single Gaussian background model. SG-Only IR the method where infrared band is modeled as a Single Gaussian. The block schema of the algorithm is given in Figure 4-28.

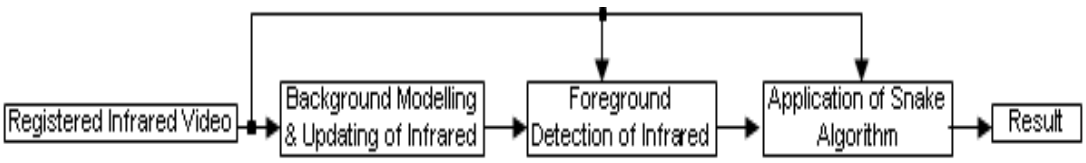

Figure 4-28 The Block Schema of the Algorithm Based on SG-IR where Only Infrared Band is Used

Since the halo effects surrounding people are more evident in our dataset, high performance can be obtained. Overall Recall value is greater than or equal to 0.95 for all background models (except SG-Only IR) which shows that our algorithm covers almost all manually segmented human regions. Precision values is greater than 0.875 for all background models (except Non-Param1) which shows that detected object from our algorithm is not scattered so much around the manually segmented human regions. For the Non-Param1 method, in some of the frames (Figure 4-33), two people are extracted as one connected component. It decreases the overall Precision value of this model. For the SG-Only IR method, because of only infrared domain is used, there exist no cues available to complete missing parts of the regions of the people (Figure 4-29). It causes low overall recall value for the model.

Table 4-3 Results of Our Algorithm: Based on Several Kinds of Background Models Obtained by Using Our Dataset

Scenes		SG-Only IR	SG	MOG	Non Param-1	Non Param-2
Scene1	Recall	0.804	0.968	0.910	0.981	0.952
	Precision	0.925	0.922	0.905	0.853	0.936
	F-Measure	0.861	0.944	0.907	0.913	0.944
Scene2	Recall	0.935	0.962	0.990	0.953	0.969
	Precision	0.875	0.888	0.766	0.809	0.893
	F-Measure	0.904	0.923	0.864	0.875	0.929
Scene3	Recall	0.749	0.926	0.943	0.946	0.950
	Precision	0.918	0.930	0.924	0.833	0.935
	F-Measure	0.825	0.926	0.933	0.886	0.942
Scene4	Recall	0.928	0.933	0.932	0.978	0.966
	Precision	0.943	0.937	0.893	0.862	0.936
	F-Measure	0.936	0.931	0.912	0.917	0.950
Scene5	Recall	0.975	0.984	0.977	0.993	0.992
	Precision	0.856	0.856	0.814	0.723	0.862
	F-Measure	0.912	0.913	0.888	0.836	0.922
Scene6	Recall	0.891	0.929	0.951	0.970	0.971
	Precision	0.959	0.960	0.952	0.825	0.946
	F-Measure	0.924	0.943	0.951	0.892	0.958
Overall	Recall	0.880	0.950	0.951	0.970	0.966
	Precision	0.913	0.916	0.876	0.817	0.918
	F-Measure	0.896	0.930	0.909	0.887	0.942

The results from each sequence are visualized below where the first row includes the tested images of infrared, color intensity, color channels and manually segmented human regions. The second row shows the output of the proposed snake algorithm. In the second row, leftmost image is based on SG-Only IR method, the next image is based on SG method, the next image is based on MOG method, the next one is based on Non-Param-1 method and the rightmost image is based on Non-Param-2 method.

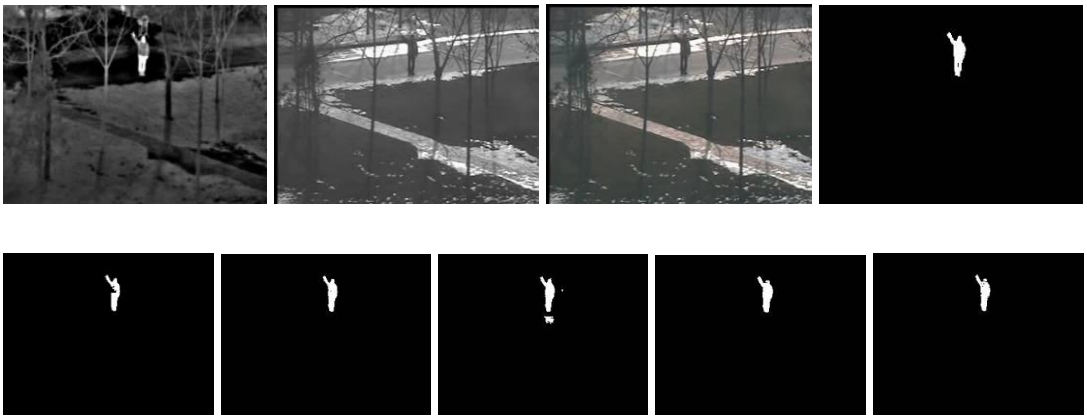

Figure 4-29 Results from Frame 1656 of Scene1 of Our Dataset

Figure 4-30 Results from Frame 373 of Scene2 of Our Dataset

Figure 4-31 Results from Frame 300 of Scene3 of Our Dataset

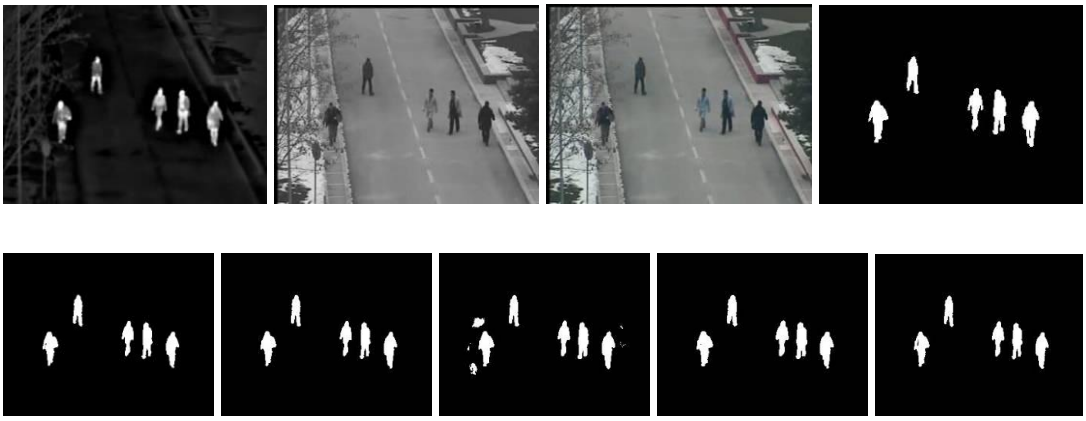

Figure 4-32 Results from Frame 1400 of Scene4 of Our Dataset

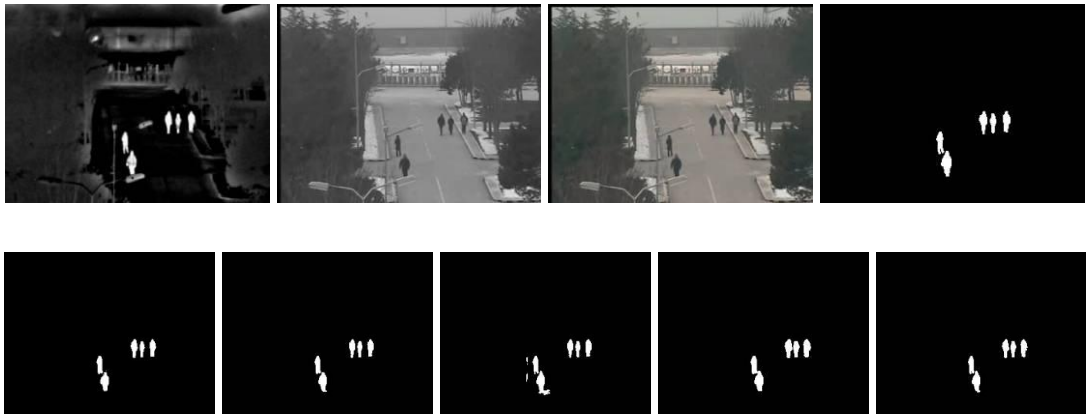

Figure 4-33 Results from Frame 1834 of Scene5 of Our Dataset

Figure 4-34 Results from Frame 1876 of Scene6 of Our Dataset

The results of our method when Single Gaussian background modelling is used where combinations of each band are represented as one vector, is shown only for a single sequence in Table 4-4. The reason of this is that highly spurious foreground regions are detected for these methods. The results based on the SG-1 model have the least spurious object and this model has highest Precision value compared to other three methods for our dataset. SG-2, SG3 and SG-4 model have higher spurious foreground regions and this affects the results as can be seen from the Table 4-4.

Table 4-4 Results of Based on Single Gaussian Methods (Combination of Bands as One Vector) Obtained by Using Our Dataset

Scenes		SG-1	SG-2	SG-3	SG-4
Scene2	Recall	0.645	0.727	0.607	0.764
	Precision	0.750	0.419	0.633	0.713
	F-Measure	0.693	0.532	0.620	0.738

The results from each sequence are visualized below where the first row includes the tested images of infrared, color intensity, color channels and manual segmented human regions. The second row shows the output of our proposed algorithm. In the second row, leftmost image is based on SG-1 method, the next image is based on SG-2 method, the next image is based on SG-3 and the rightmost image is based on SG-4 method.

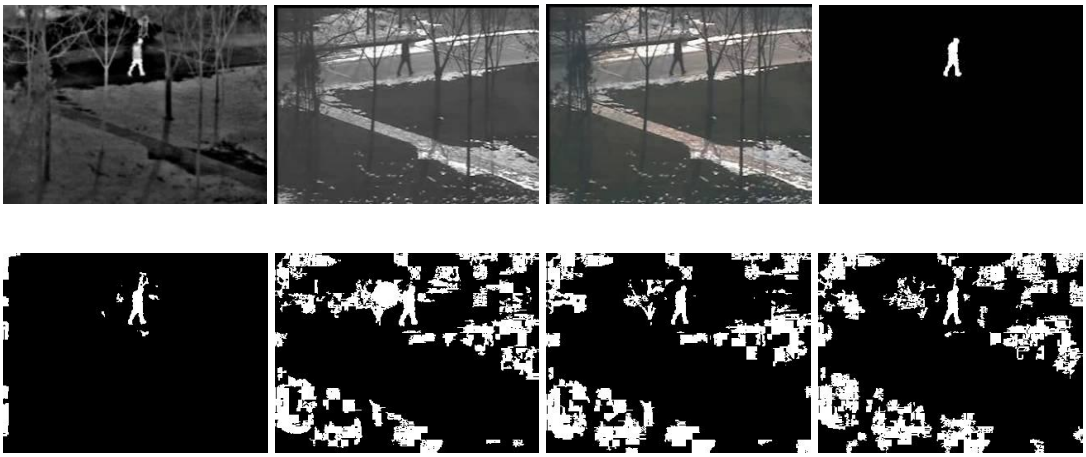

Figure 4-35 Results from Frame 373 of Scene2 of Our Dataset

CHAPTER 5

SUMMARY AND CONCLUSIONS

In this thesis, detection of foreground objects, especially people, is performed using synchronized and registered infrared and visual images all together. Sudden illumination changes and shadows do not generally affect the background model in infrared domain. The temperature of the background is more stable over time and operation of all around the day is valid in infrared domain. These are the main reasons that the initial regions of interest are found firstly in infrared domain and these regions are used as a mask in the visible domain. However, some object regions may not be detected from infrared image due to the fact that the temperature of the foreground objects may be very close to the background model. Thus, after finding the corresponding foreground regions in visible domain, addition of the visible cues (if available) to foreground regions of infrared domain is performed. As a result, the missing regions are complete on the thermal foreground mask using corresponding visual information. Finally, application of snake algorithm to the current infrared image, which is masked with the constructed foreground regions, gives very successful results for people detection. Results are more robust when the halo effects surrounding the people are more evident.

Performance of the proposed algorithm is tested with two datasets (OTCBVS benchmark and our dataset) each of which includes six challenging sequences. For each sequence, 10 frames are chosen and segmented manually. To show applicability of our algorithm for various sequences, all parameters/thresholds

are fixed before tests. The quantitative performance is demonstrated by precision and recall parameters. The results are compared also with the results given in [1] by using the OTCBVS benchmark. Although these sequences have weaker halo effects which surround the people, promising results are derived. In all sequences our recall values are higher but the precision values are smaller than the ones expressed in [1]. This means that we detect more of the actual regions. In our dataset, halo effects are more evident and in these sequences we obtain better results. Various background modeling methods have been used for this purpose. Effects of these methods to human detection performance are also given in Section 4.5.

Object identification will be the topic of future research. For example, some basic parameters like area of the blob, height to width ratio etc. will be used to eliminate non-human objects. If clear human silhouettes could be extracted, further tasks such as activity recognition could also be studied.

REFERENCES

[1]: J. W. Davis, and V. Sharma. “Background-subtraction using contour-based fusion of thermal and visible imagery”. In *Computer Vision and Image Understanding* 106(2-3): 162-182, 2007.

[2]: C. O. Conaire, E. Cooke, N. O’Connor, N. Murphy, and A. Smeaton. “Background modelling in infrared and visible spectrum video for people tracking”. In *Proc. IEEE Conf. on Computer Vision and Pattern Recognition Workshop*,page 20, Washington, DC, USA, 2005.

[3]: A. Elgammal, D. Harwood, and L. Davis. “Non-parametric model for background subtraction”. In *Proceedings of the 6th European Conference on Computer Vision*, 2000.

[4]: A. Leykin, Y. Ran, and R. Hammoud, “Thermal-visible video fusion for moving target tracking and pedestrian classification”. In *Computer Vision and Pattern Recognition*, 2007. *CVPR '07. IEEE Conference on* 17-22 June 2007 Page(s):1 - 8

[5]: K. Kim, T. H. Chalidabhongse, D. Harwood, and L. Davis. “Background modeling and subtraction by codebook construction”. In *International Conference on Image Processing*, 2004.

[6]: A. Leykin and M. Tuceryan. “A vision system for automated customer tracking for marketing analysis: Low level feature extraction”. In *Human Activity Recognition and Modelling Workshop*, 2005.

[7]: Y Ran, I. Weiss, Q. Zheng, and L. S. Davis: “Pedestrian detection via periodic motion analysis”. In *International Journal of Computer Vision* 71(2): 143-160 (2007)

[8]: I. Haritaoglu, D. Harwood, and L.S. Davis, “W4: real-time surveillance of people and their activities”. In *IEEE Transactions on Pattern Analysis and Machine Intelligence*, Vol. 22, No. 8, pp. 809-830, 2000.

[9]: L. Zhang, B. Wu, and R. Nevatia. “Pedestrian detection in infrared images based on local shape features”. In *the 4-th Joint IEEE International Workshop on Object Tracking and Classification in and Beyond the Visible Spectrum (OTCBVS'07),* in conjunction with CVPR 2007

[10]: N. Dalal and B. Triggs. “Histograms of oriented gradients for human detection”. In *Coference on Computer Vision and Pattern Recognition (CVPR),* 2005.

[11]: C. Dai, Y. Zheng, and X. Li. “Layered representation for pedestrian detection and tracking in infrared imagery”. In *IEEE CVPR WS on OTCBVS*, 2005.

[12]: J. Zhou and J. Hoang. “Real time robust human detection and tracking system”. In *IEEE Computer Society Conference on Computer Vision and Pattern Recognition*, 3:149 – 149, 2005.

[13]: M. Hussein, W. Abd-Almageed, Y. Ran, and L. Davis: “Real-time human detection, tracking, and verification in uncontrolled camera motion environments”. In *International Conference on Computer Vision Systems* ICVS 2006

[14]: G. Wolberg and S. Zokai. “Robust image registration using log-polar transform”. In *International Conference on Image Processing*, 2000.

[15]: D. Gavrila. “Pedestrian detection from a moving vehicle.”. In *ECCV ’00: Proceedings of the 6th European Conference on Computer Vision-Part II*, pages 37–49, London, UK, 2000. Springer-Verlag.

[16]: S. K. Zhou, R. Chellappa, and B. Moghaddam. “Visual tracking and recognition using appearance-adaptive model in particle filters”. In *IEEE Transactions on Image Processing*, 13(11):1491–1506, November 2004.

[17]: R. Fletcher (Ed.), “Practical Methods of Optimization”, *Wiley, New York*, 1990.

[18]: H. G. Barrow. “Parametric correspondence and chamfer matching: two new techniques for image matching.”. In *International Joint Conference on Artificial Intelligence*, pages 659–663, 1977.

[19]: W. E. L. Grimson and C. Stauffer, “Adaptive background mixture models for real-time tracking.”. In *Proc. IEEE Conf. CVPR*, Vol. 1, pp 22-29, 1999.

[20]: P. KadewTraKuPong and R. Bowden, "An improved adaptive background mixture model for real-time tracking with shadow detection". In *Proc. 2nd European Workshp on Advanced Video-Based Surveillance Systems*, 2001

[21]: T. Chan and L. Vese, “Active contours without edges.”. In *IEEE Trans. ImageProcessing*, 10(2):266–277, Feb. 2001.

[22]: O. Javed, K. Shafique, and M. Shah. “A hierarchical approach to robust background subtraction using color and gradient information.”. In *Workshop on Motion and Video Computing*, pages 22-27, Dec 2002

[23]: T. Horprasert, D. Harwood, and L.S. Davis “A *statistical approach for real-time robust background subtraction and shadow detection*.”. In *IEEE ICCV'99 FRAME-RATE WORKSHOP*. 1999.

[24]: http://www.engr.uconn.edu/~cmli

[25]: http://www.cse.ohio-state.edu/otcbvs-bench

[26]: J. Davis and V. Sharma. “Robust background-subtraction for person detection in thermal imagery”. In *IEEE International Workshop on Object Tracking and Classification Beyond the Visible Spectrum*, 2004.

[27]: J. Davis and V. Sharma. “Robust detection of people in thermal imagery”. In: *Proceedings on International Conference on Pattern Recognition*, 2004, pp. 713–716.

[28]: D. Mumford and J. Shah. “Optimal approximation by piecewise smooth functions and associated variational problems” In *Commun. Pure Appl. Math*, vol. 42, pp. 577–685, 1989

[29]: N. Oliver, B. Rosario, and A. Pentland. “A Bayesian Computer Vision System for Modeling Human Interactions”. In *International Conference on Vision Systems*, 1999.

[30]: Y.L.Tian and A.Hampapur. “Robust Salient Motion Detection with Complex Background for Real-time Video Surveillance”, In *Proc. Of IEEE Computer Society Workshop on Motion and Video Computing*, January, 2005